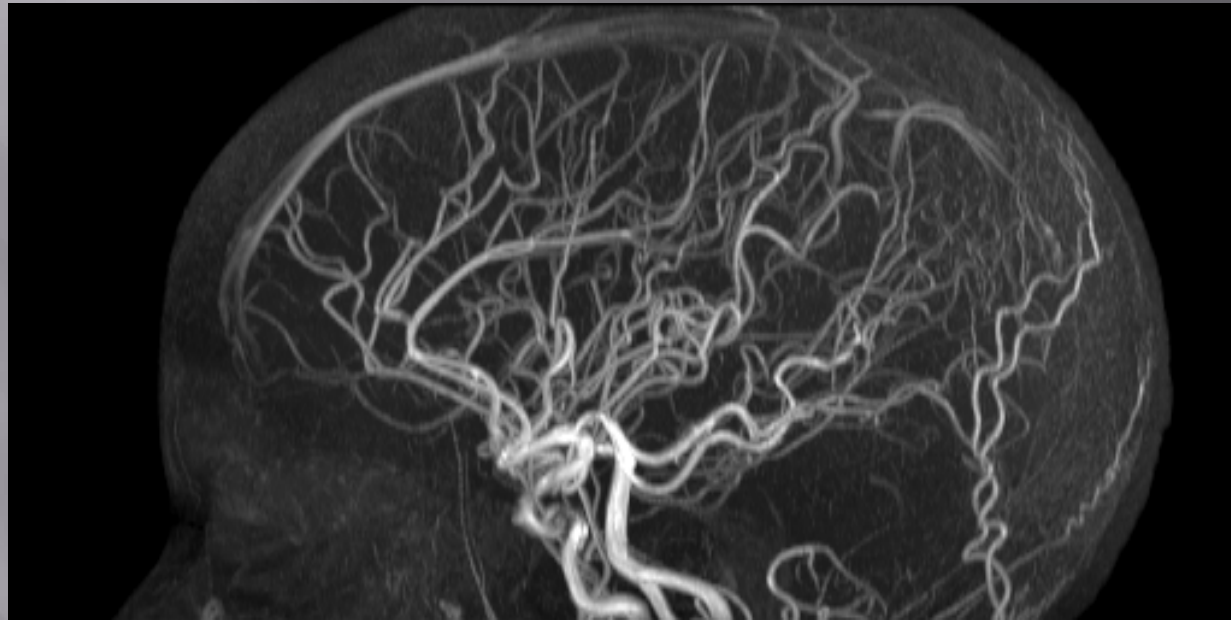


The application of SWI and SWIM in imaging stroke, traumatic brain injury and tumors



E. Mark Haacke, PhD, nmrimaging@aol.com
Director, MR Research Facility, Wayne State University
Detroit, Michigan

Disclosures

I am affiliated with:

Wayne State University

McMaster University

The MRI Institute for Biomedical Research

and have an interest in

MR Innovations, Inc.

and have support from

Siemens Healthcare and

The National Institutes of Health

Acknowledgements

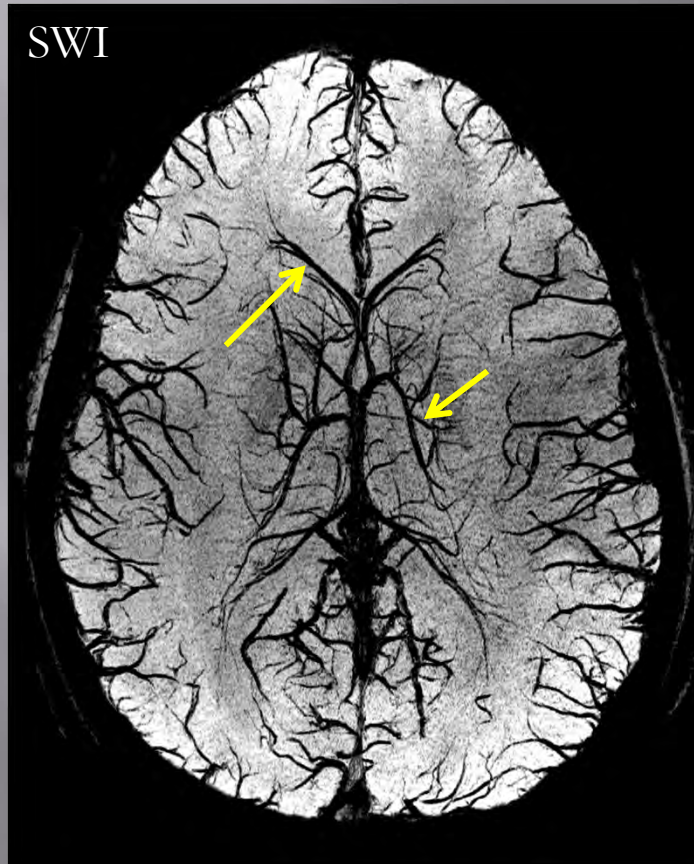
- ▣ Xia Shuang, Tianjin, stroke
- ▣ Liu Jiangtao, headache
- ▣ David Hubbard, MD for MS data
- ▣ Joseph Hewett, MD for MS data
- ▣ Wei Feng, PhD for processing flow data
- ▣ Gabriele Trifan, MD for image analysis
- ▣ David Utriainen, for image analysis
- ▣ Sean Sethi, MS, for image analysis
- ▣ Giacomo Gadda, for image analysis
- ▣ Meng Li, MS, for perfusion TSM data
- ▣ Jaladhar Neelavalli, PhD for SWIM support
- ▣ Zhifeng Kou, PhD for TBI data

Informational Websites

- ▣ Clinical applications of SWI and SWIM
- ▣ See www.swim-mri.com

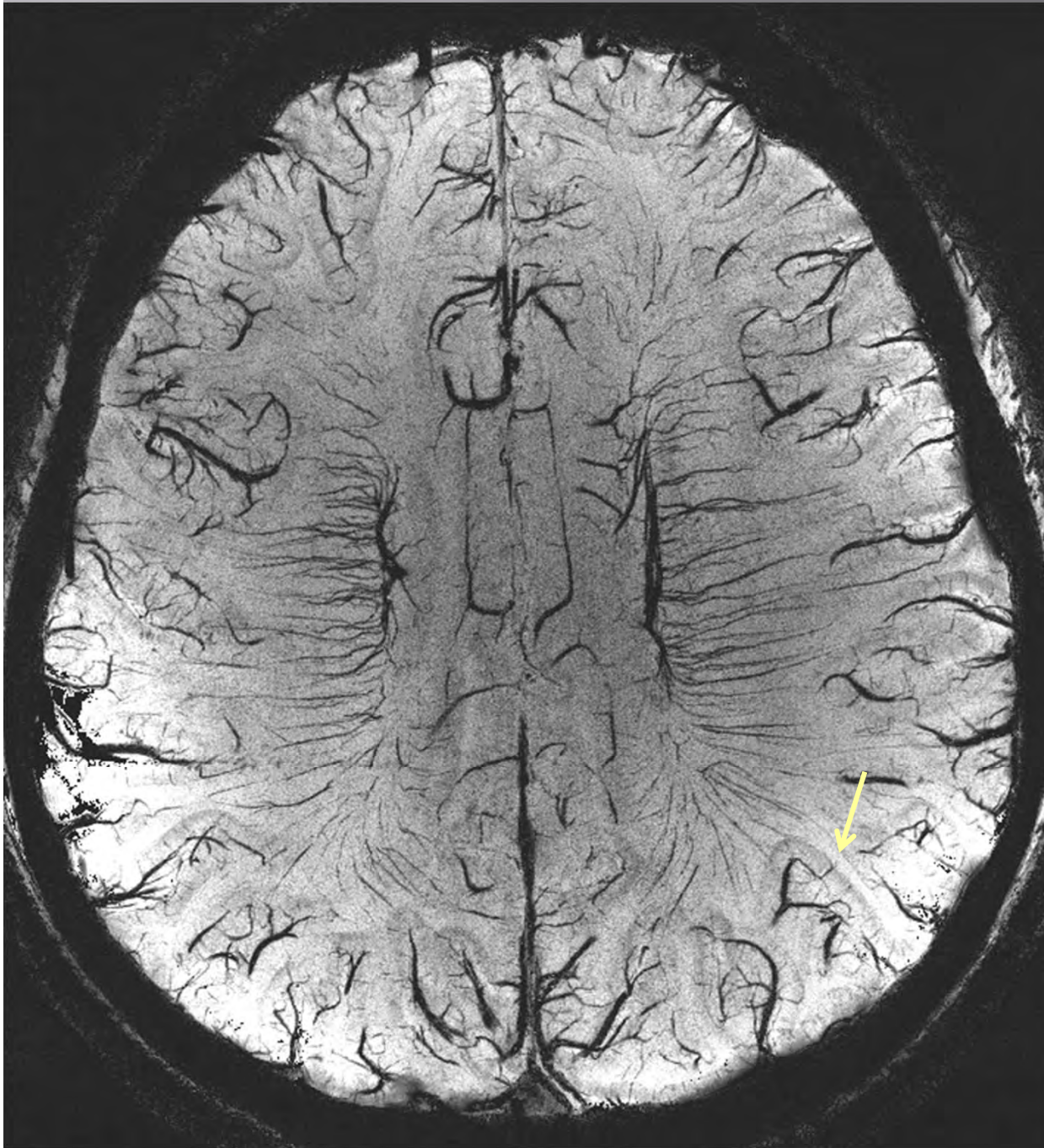
- ▣ The role of abnormal venous flow in neurodegenerative diseases: MS as an example
- ▣ See www.ms-mri.com
- ▣ Our work in Detroit at Wayne State University
- ▣ See www.mrc.wayne.edu

Susceptibility Weighted Imaging



- Enhances the presence of ferritin, hemosiderin and deoxyhemoglobin
- Exquisite images from which brain damage, microbleeding and increases in deoxyhemoglobin can be diagnosed

Haacke EM et al. Susceptibility weighted imaging. *Magnetic Resonance in Medicine*, 52: 612; 2004.



7T SWI

$215\mu \times 215\mu \times 1000\mu$

TE = 16ms

TR = 45ms

FA = 25°

8 slice mIP

Image courtesy of Yulin Ge
New York University

High resolution MR angiography



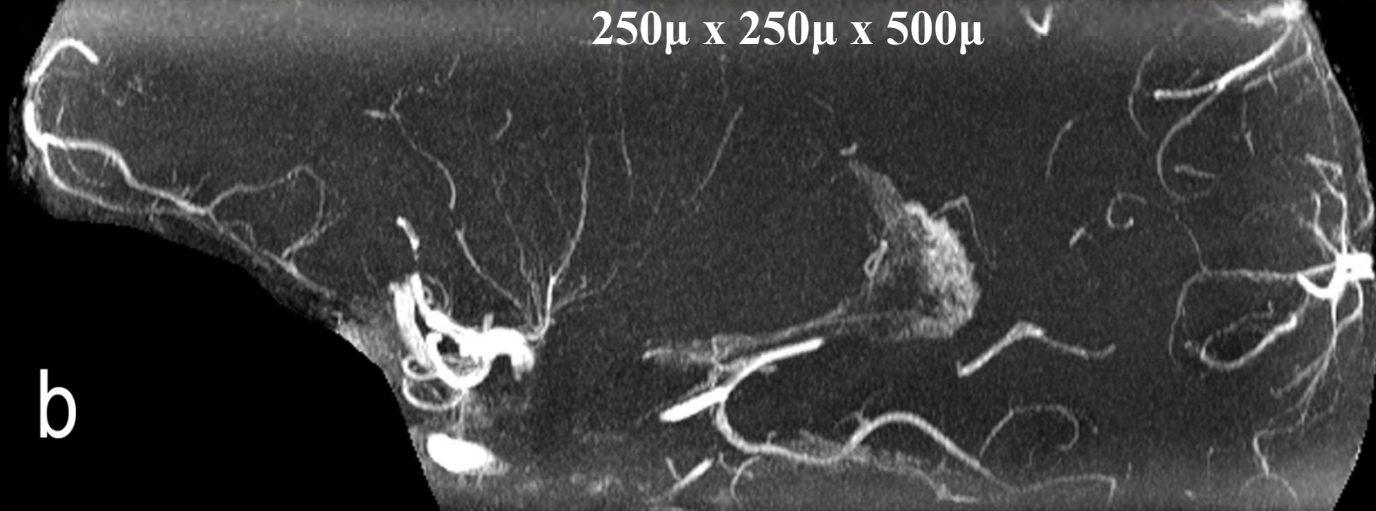
11) Salamon, G., 1971. Atlas of the arteries of the human brain. Sandoz, Paris.

a

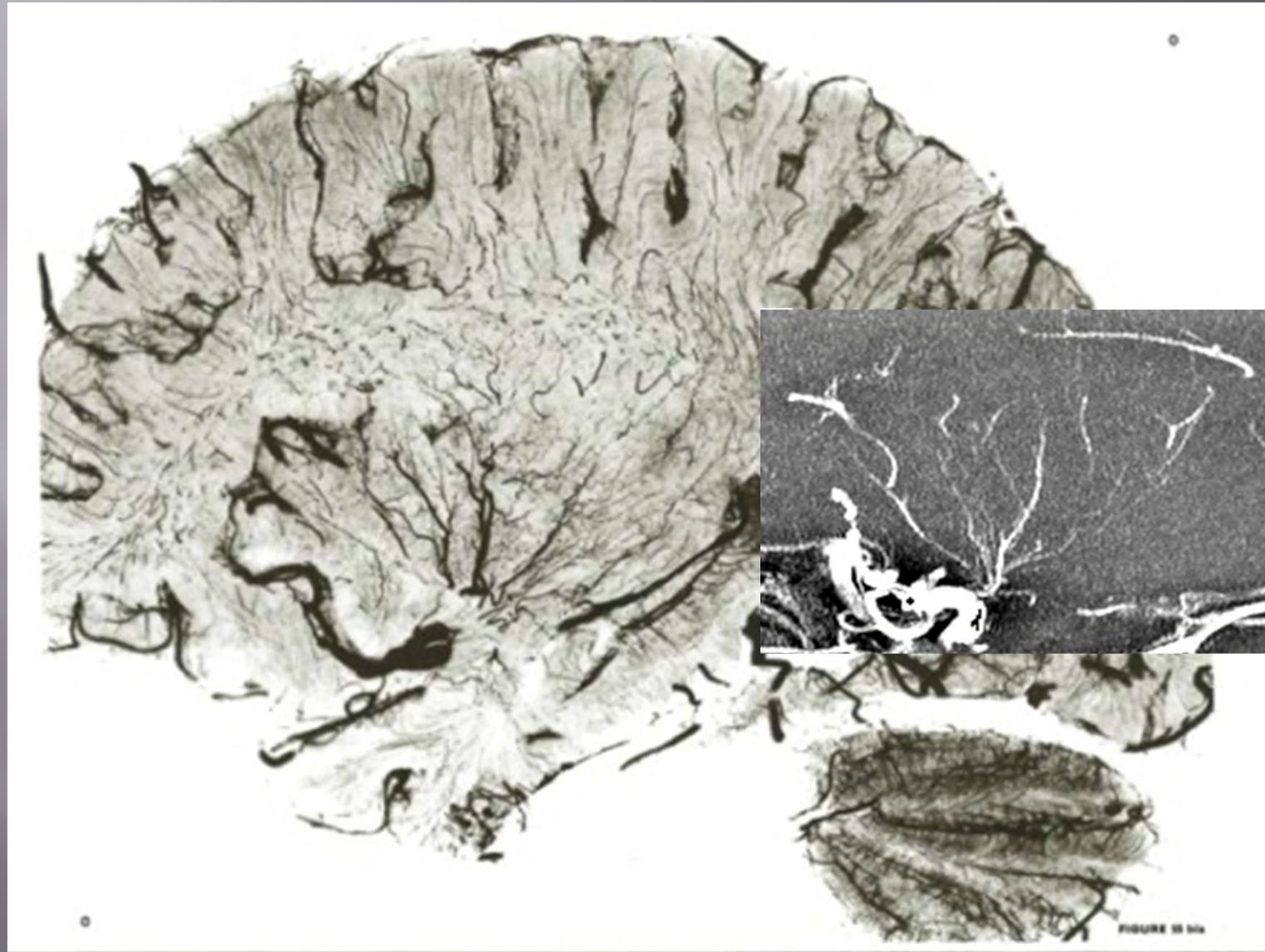


250 μ x 250 μ x 500 μ

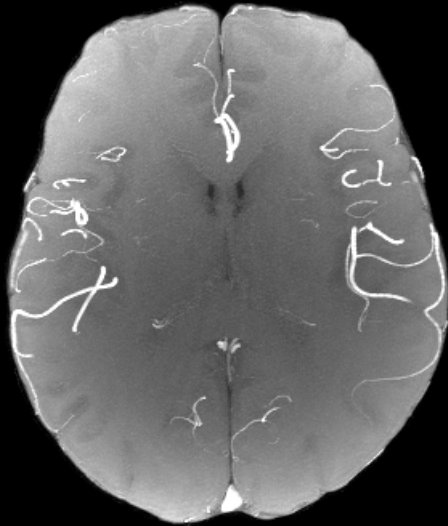
b



Small arteries around 250 microns and possibly even smaller are becoming visible



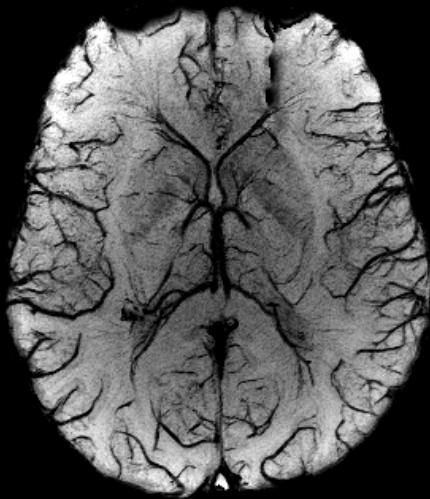
MRA short echo SWI



RP-DP MRA



SWI only veins



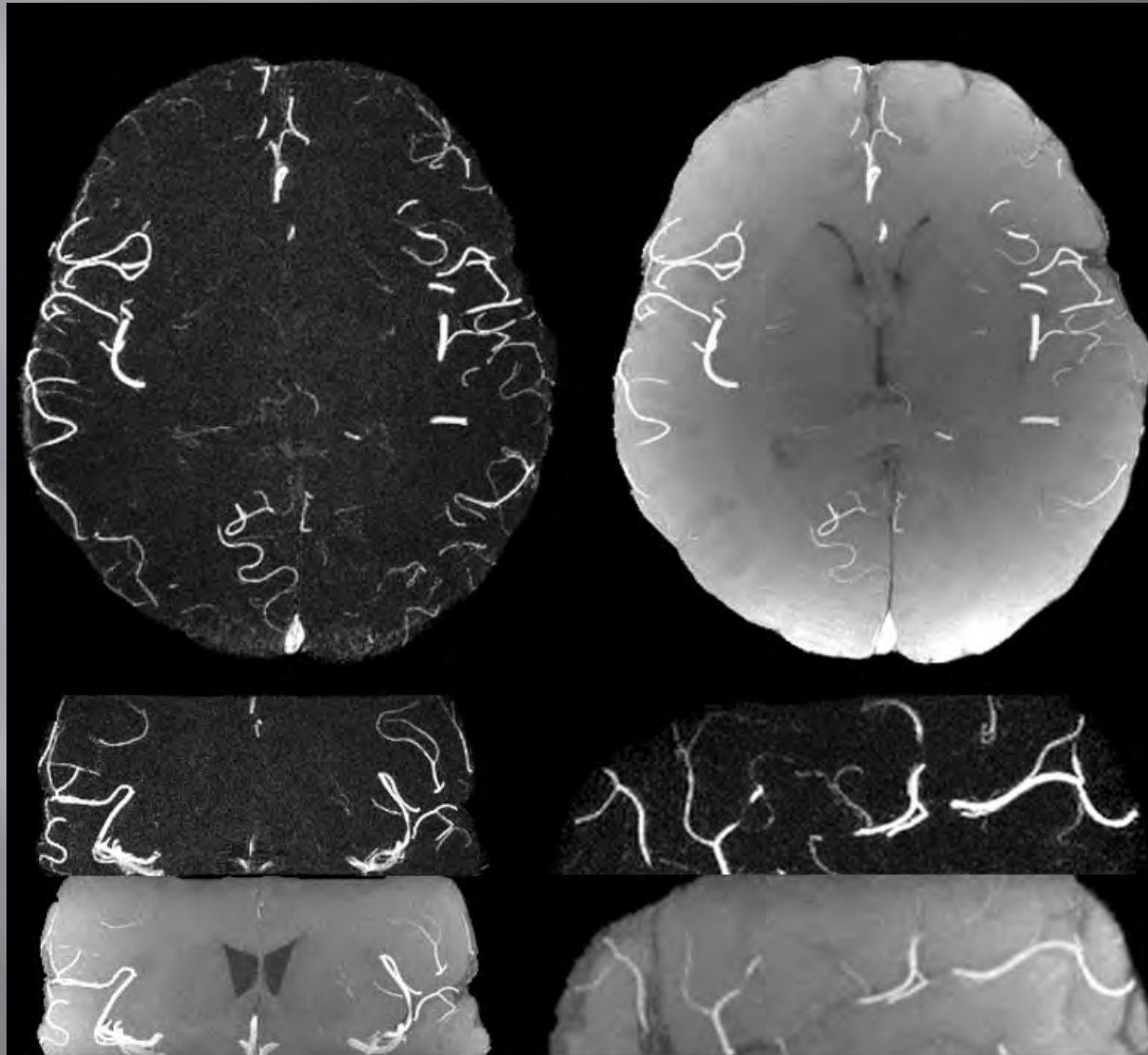
RP-DP MRA



Simultaneous MRV and MRI using a double echo interleaved SWI rephased/dephased sequence⁷

At 3T, veins are more naturally suppressed because they have $T2^* = 25\text{ms}$ while arteries have a $T2^*$ closer to 70-80ms. Images acquired with a resolution of 0.5mm x 0.5mm in-plane and 1mm thick slice. 0.5mm in-plane resolution.

Images courtesy of Yongquan Ye, PhD



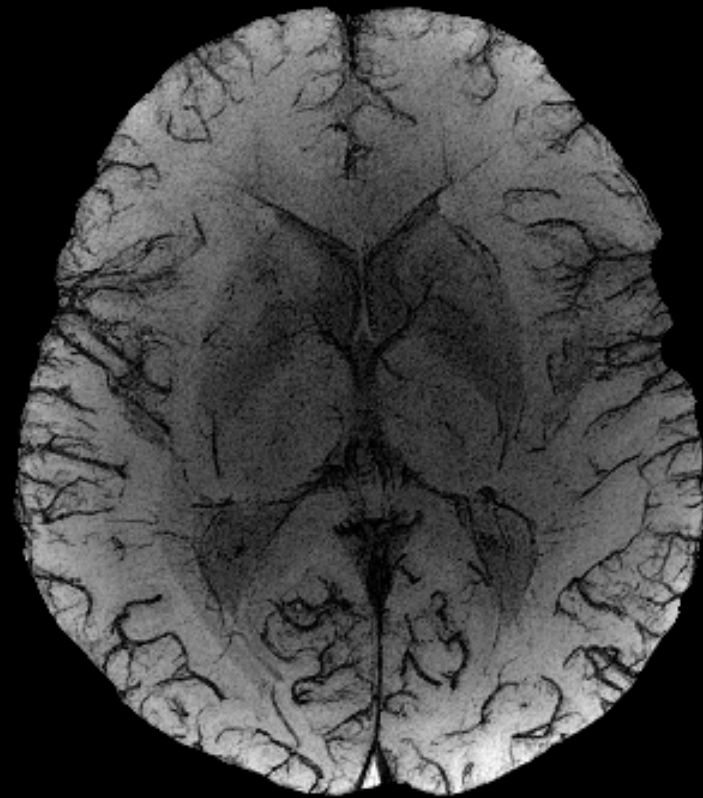
Comparison of 2nd TE (FR-FD) and 1st TE MRA

3D MRAV of the brain

Simultaneous MRV and MRA using a double echo
interleaved SWI rephrased(FR)/
dephased(FD) sequence



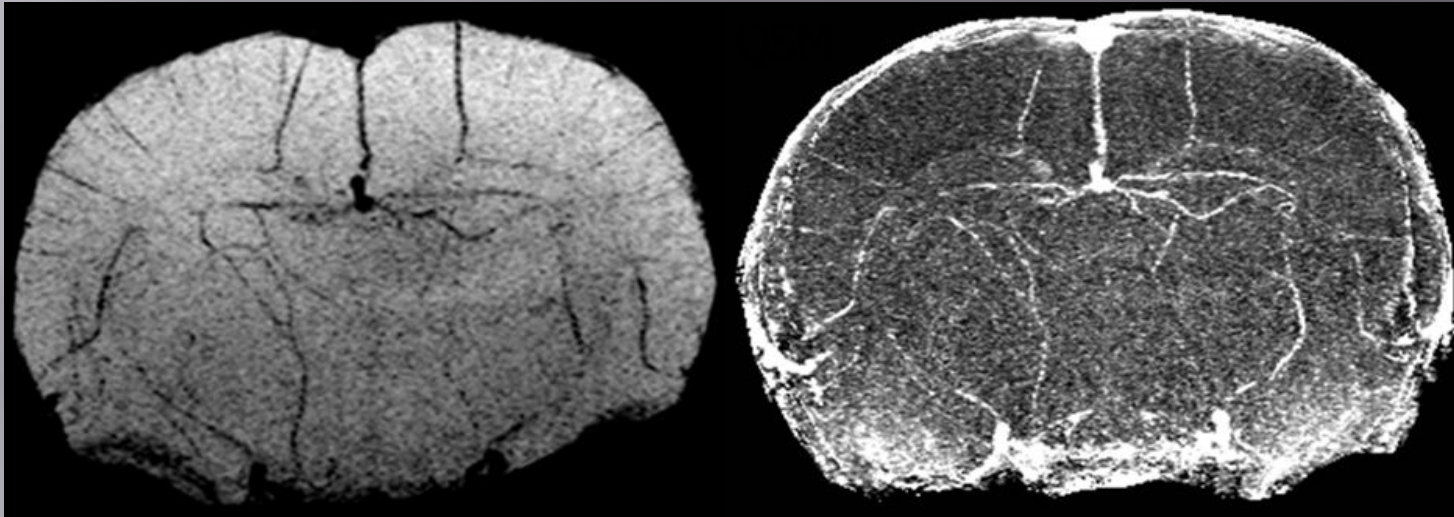
1st TE FR – 2nd TE FD



SWI like mIP

SWI: Future Directions

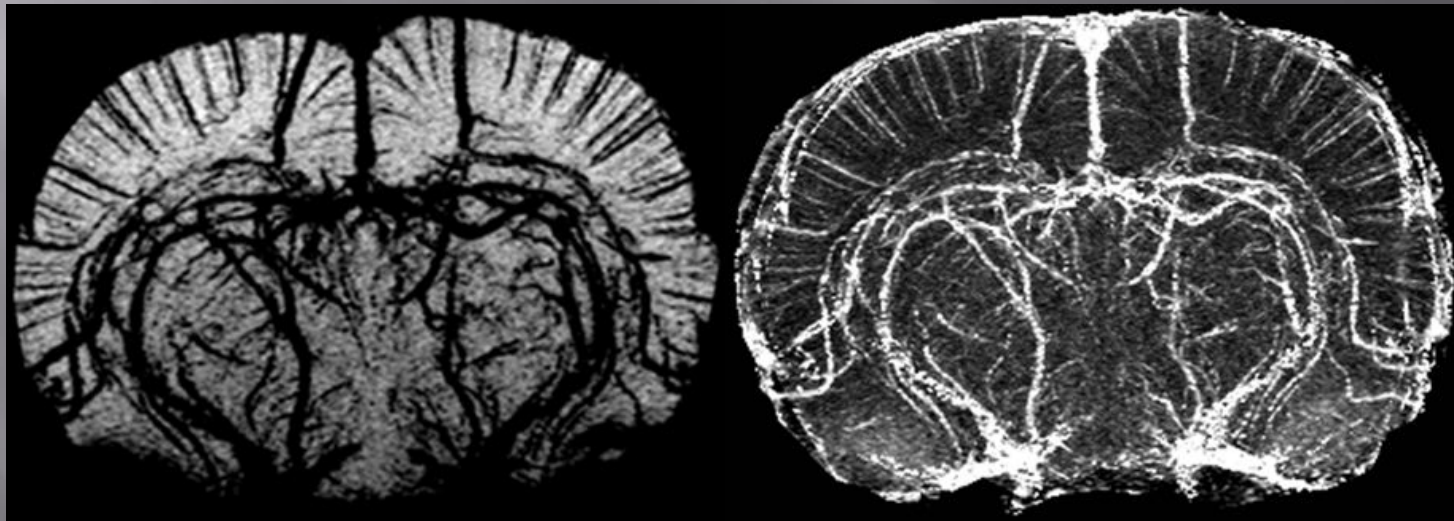
*Past
20
Years*



SWI of arteries with P904

QSM of arteries with P904

*Future
20
Years*



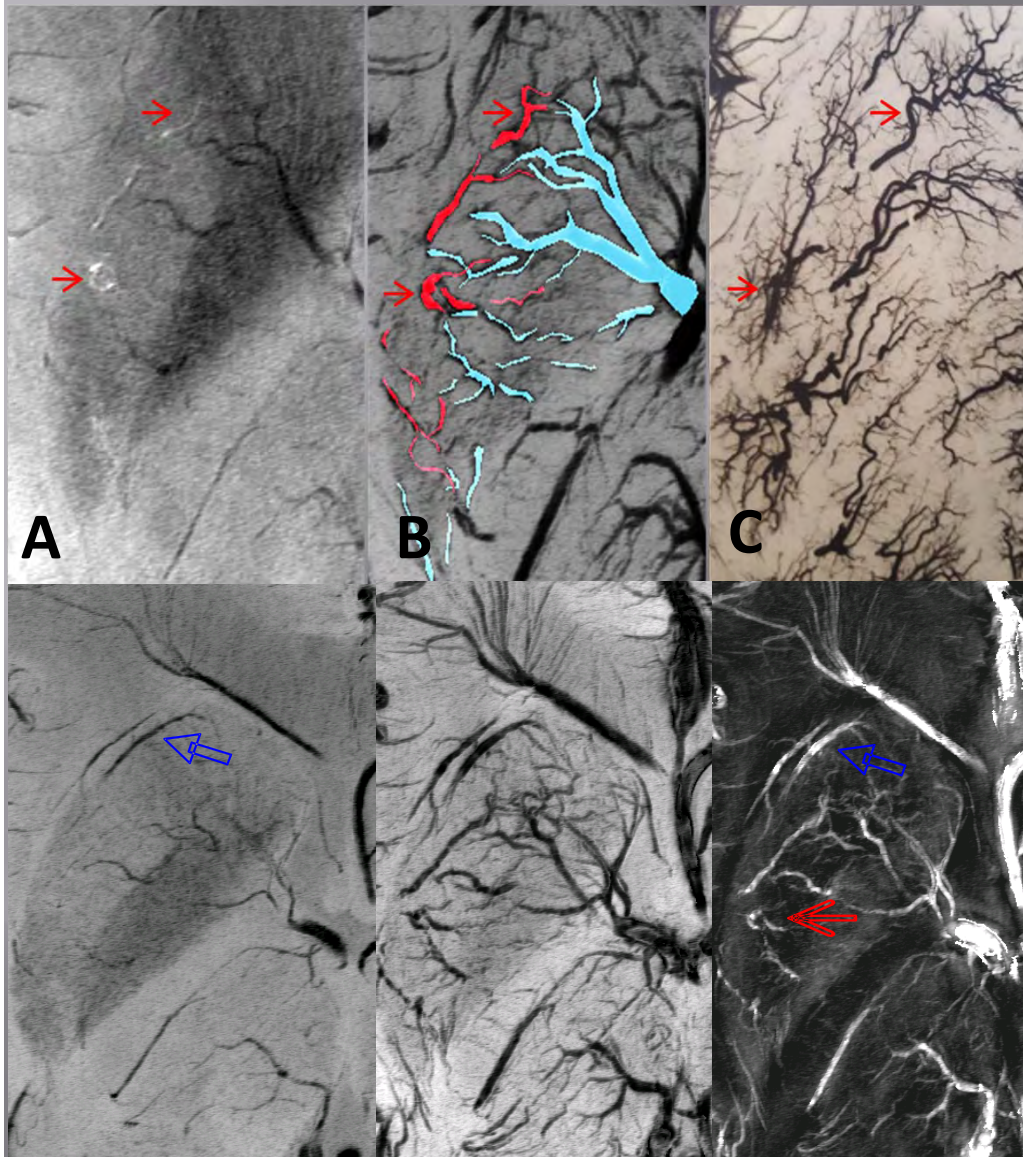


Figure 3. MICRO data acquired at 7T with TE = 8ms and a resolution of 100 μ m x 200 μ m x 1.25mm.

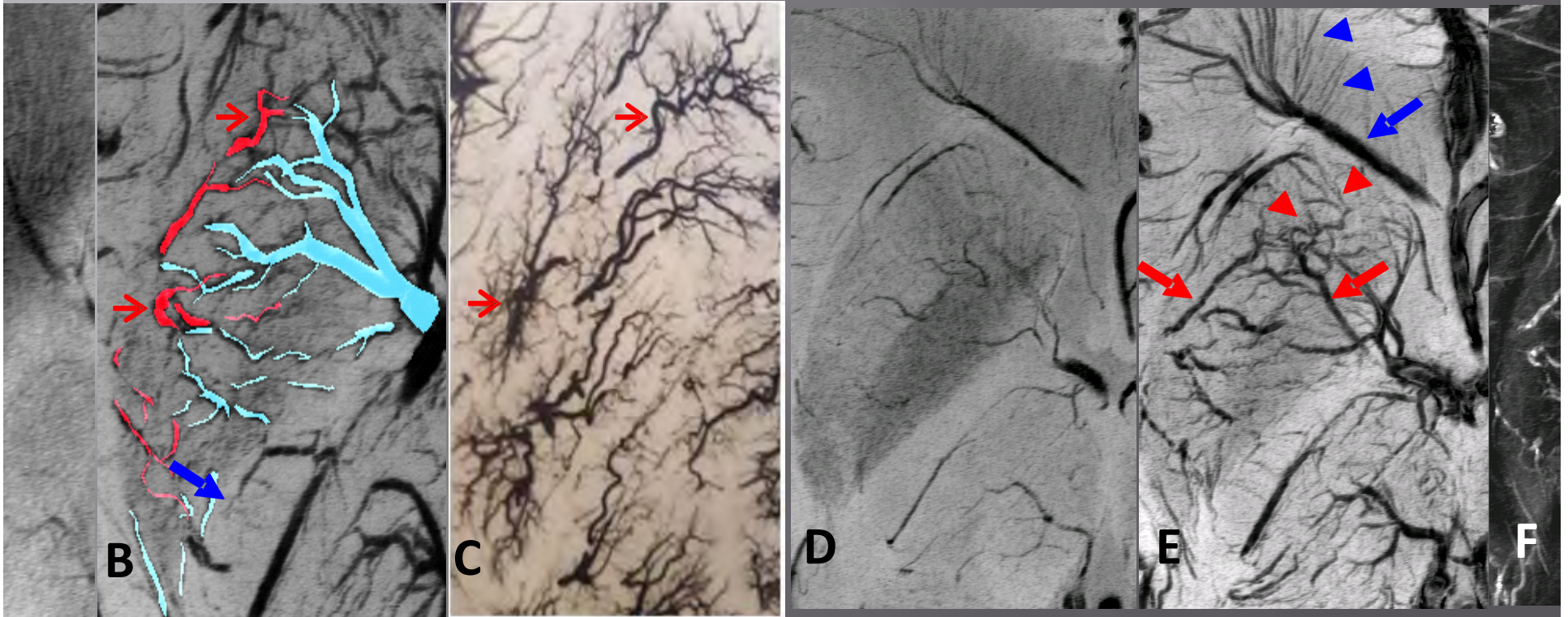
- (A) MIP of pre-contrast original magnitude image (1st echo) showing the arterial signal (red).
- (B) Post 4mg/kg Ferumoxytol MICRO image.
- (C) Basal ganglia arteries from the cadaver brain work of Georges Salamon (1971).
- (D) mIP of pre-contrast SWI shows veins only.
- (E) Post-Ferumoxytol SWI (2mg/kg) showing both veins and arteries including small arterioles (red arrowheads) and venules (blue arrowheads).
- (F) Post-contrast QSM showing higher susceptibility values in veins than in arteries.

Our goal is to track both arteries and veins, and use this to study microvascular disease at 3T.

Arteries, arterioles and venules are now visible thanks to the susceptibility contrast and blooming effect from Feuromxytol.

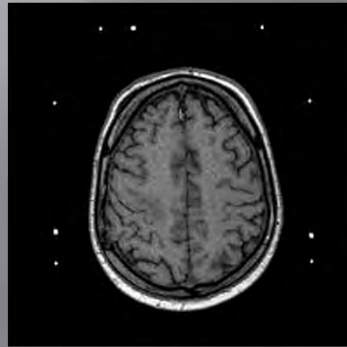
The process of separating arteries from veins from pre/post Ferumoxytol images.

The process of separating arteries from veins from pre/post Ferumoxytol images.

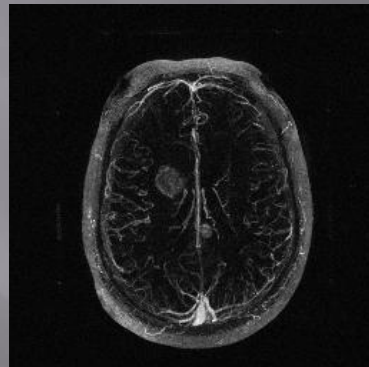
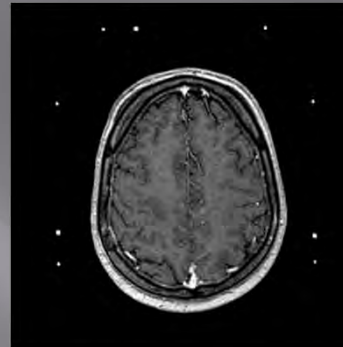


CONTRAST ENHANCED TUMOR IMAGING 3D T₁ WEIGHTED

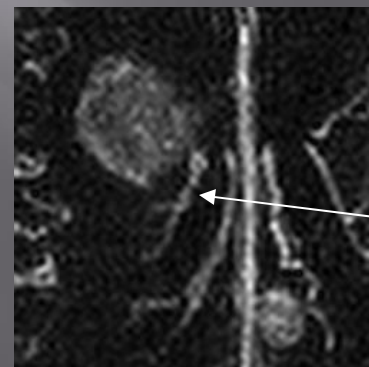
Flash 3D T₁
weighted pre-
Gadolinium
series



Flash 3D T₁
weighted post-
Gadolinium
series



T₁ subtraction
maximum
intensity
projection image

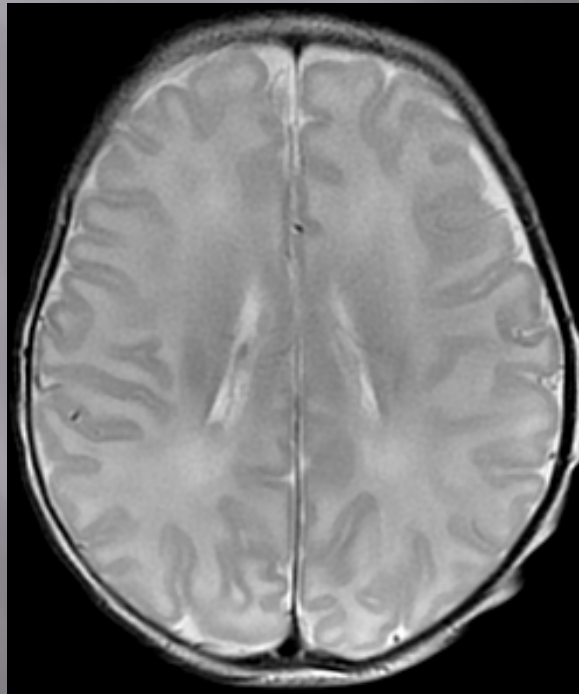


Tumor
draining/feeding
vessels

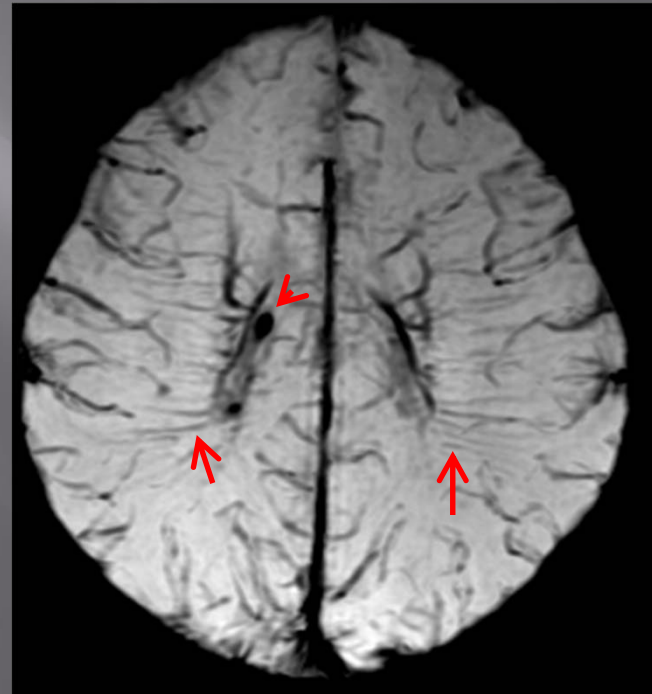
The 3D sequence allows better coverage of the tumor volume and pre-post contrast imaging allows exact subtraction revealing enhanced regions and in some cases even feeding/draining vessels.

SWI- Venography in Pediatric Population

2 day old infant

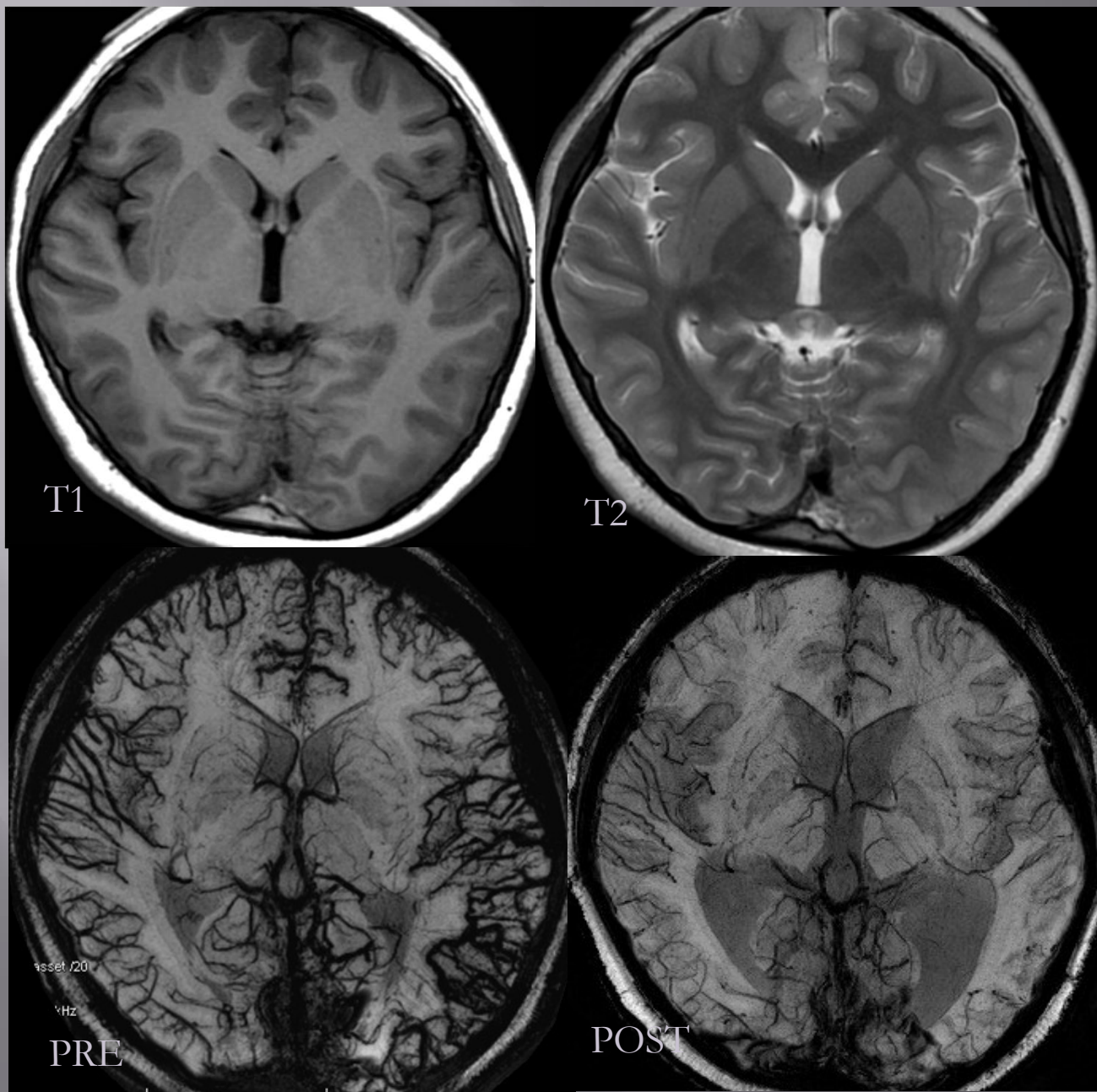


T2



SWI

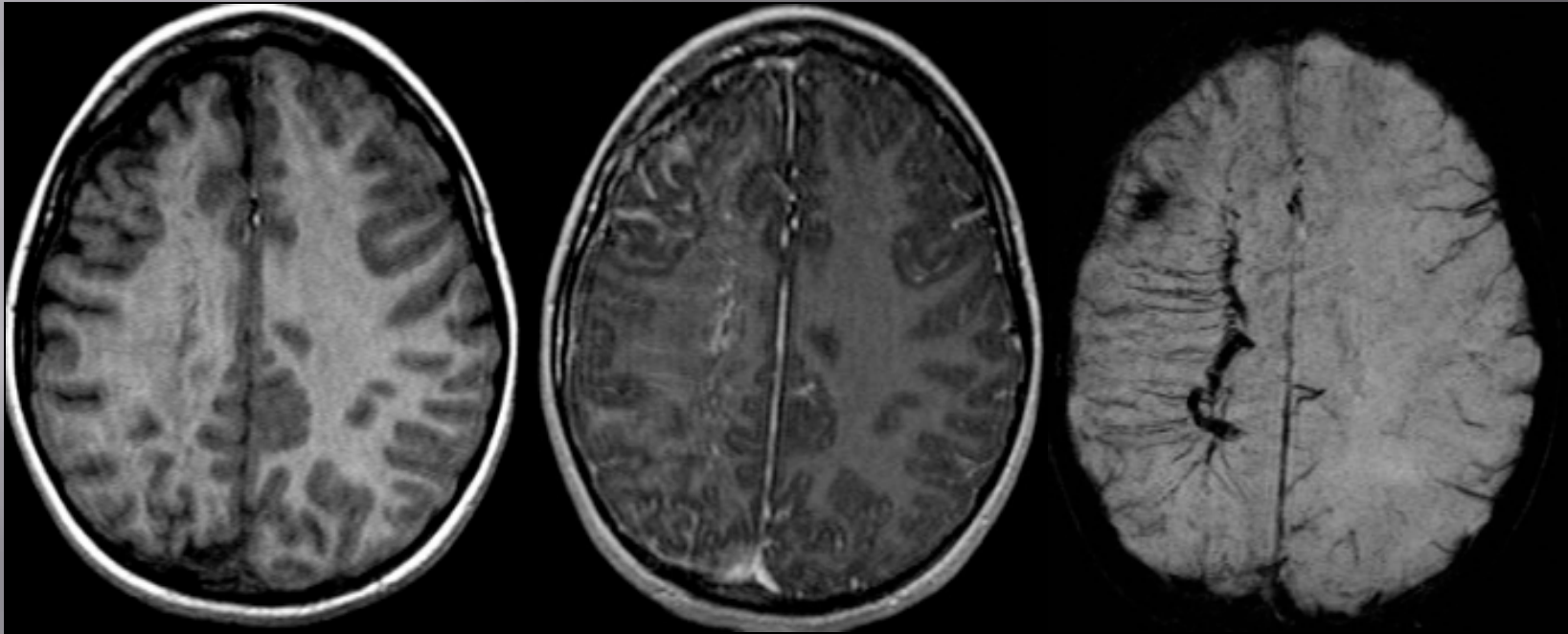
Neonatal encephalopathy



Venous Thrombosis: before treatment and after thrombolysis

Guangbin Wang M.D.
Shandong Medical
Imaging Research
Institute

Sturge Weber Syndrome

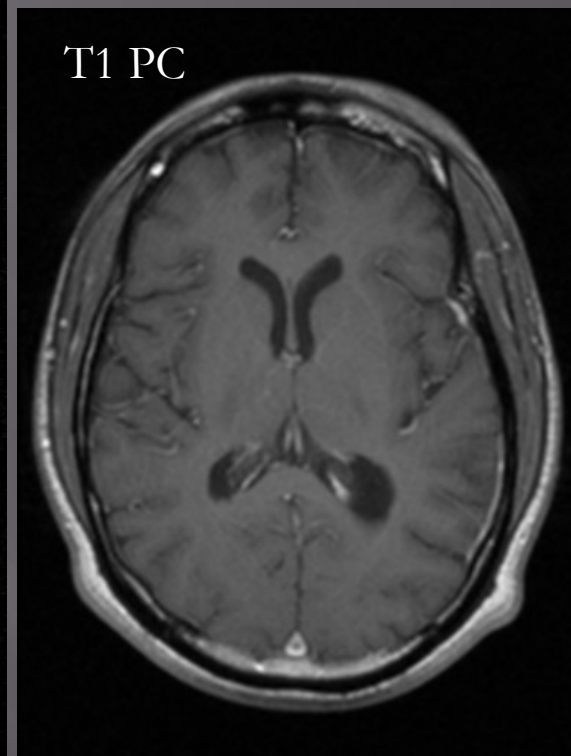
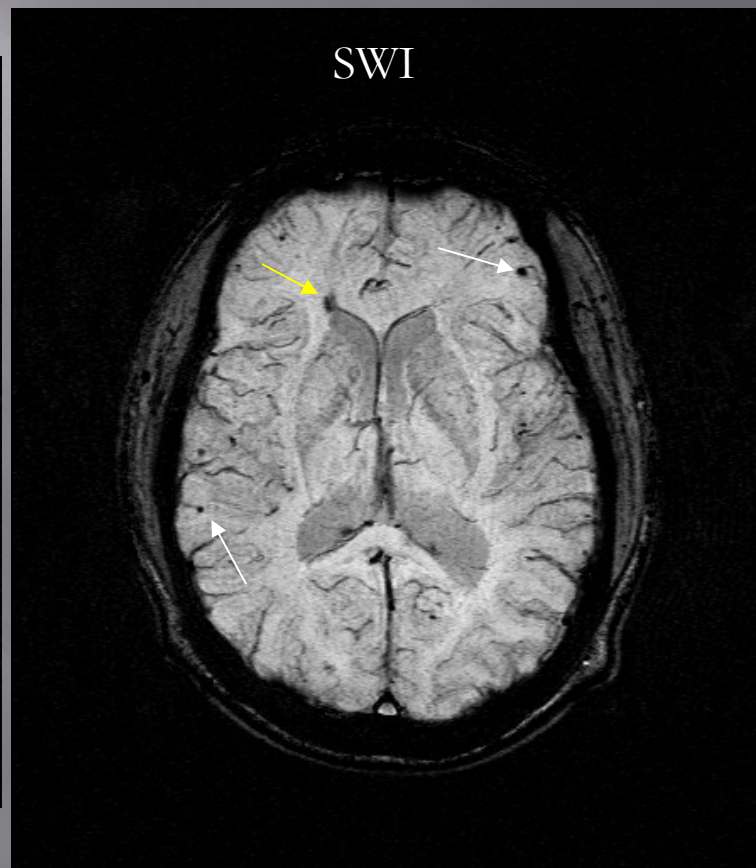
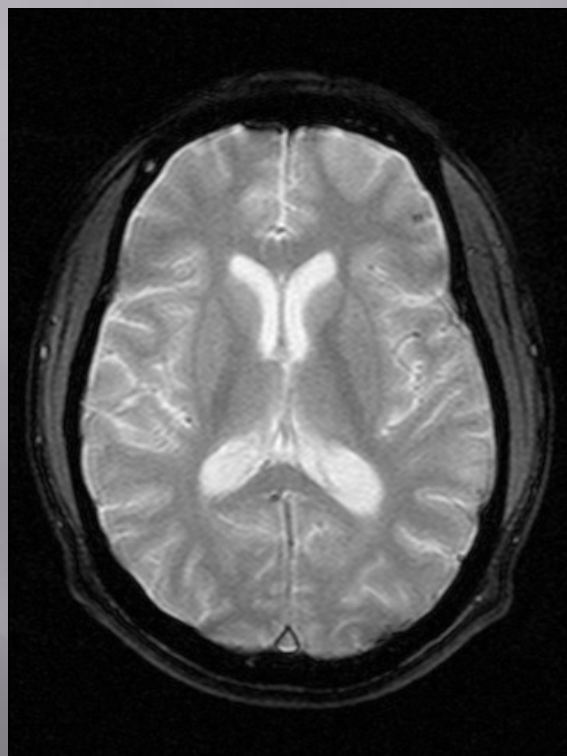


3D-T1

Post Gd 3D T1

SWI (no contrast agent)

Motorcycle trauma: medullary vein involvement

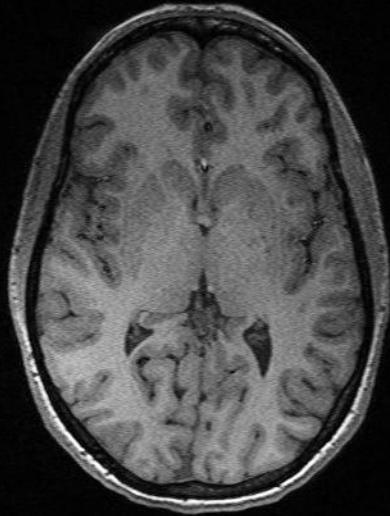


Medullary vein involvement

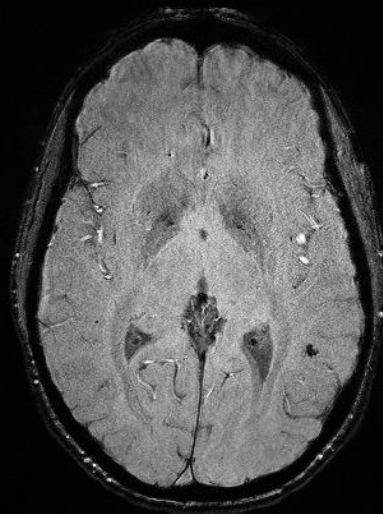
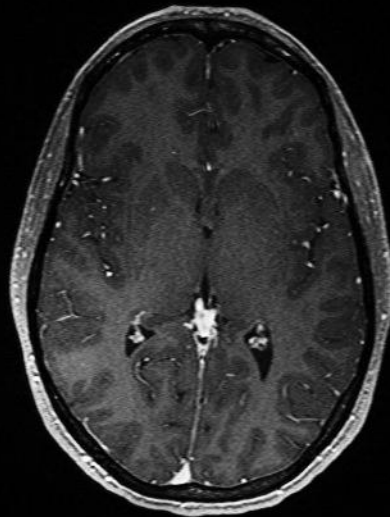
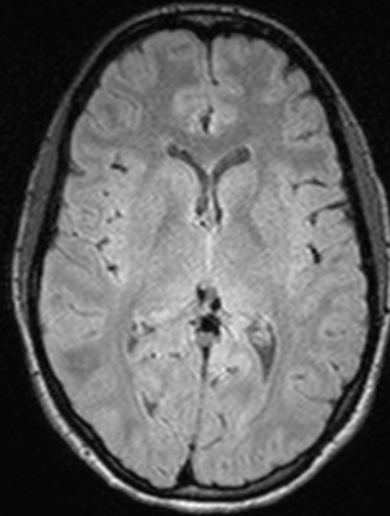


Z. Kou et al. The Role of Advanced MR Imaging Findings as Biomarkers of Traumatic Brain Injury (TBI). *J. Head Trauma Rehabil.* 2010 - 25:267-282.

T1 pre contrast

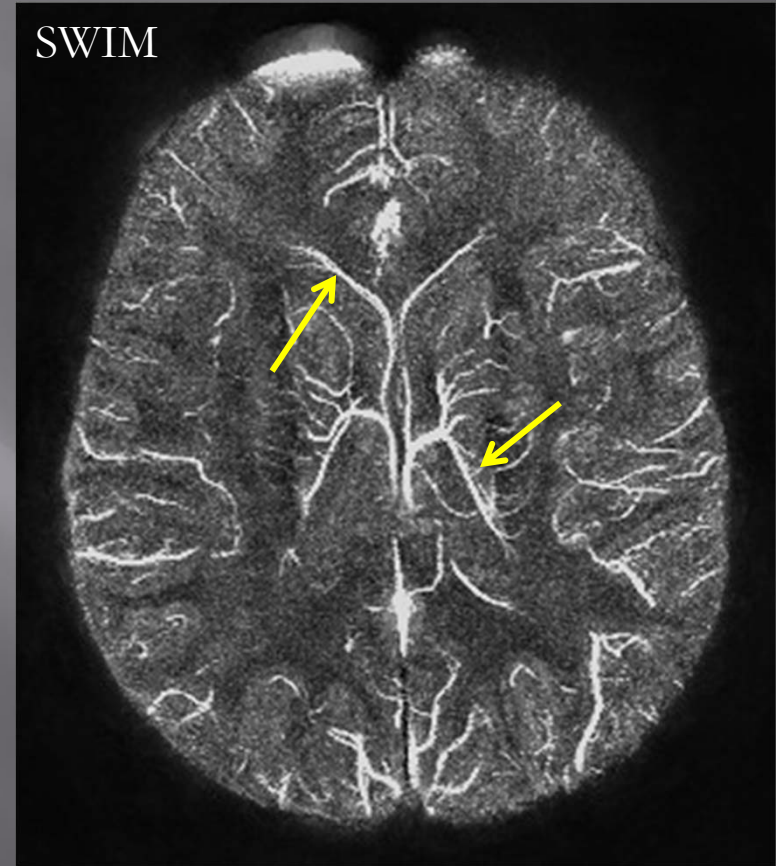
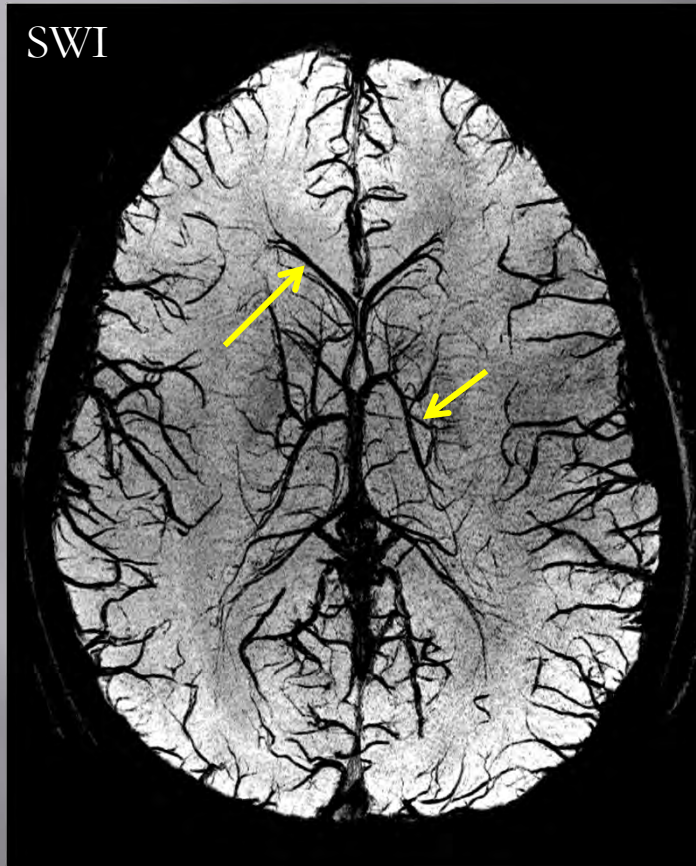


FLAIR



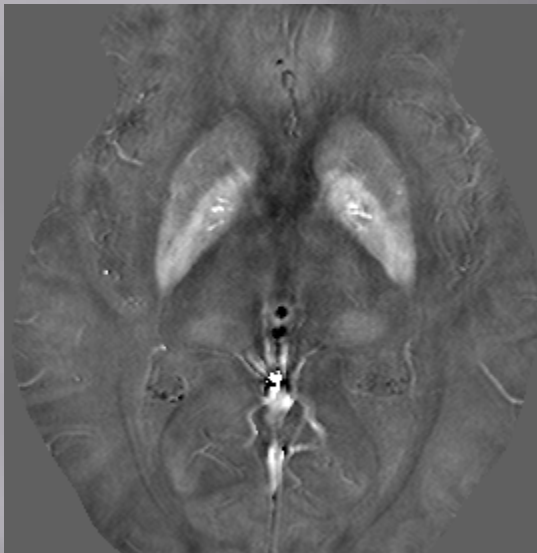
**SEIZURE
CASE**

SWI vs. SWIM

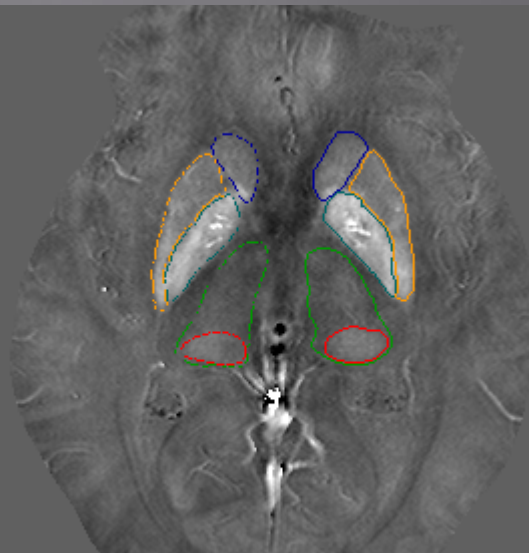


- SWI enhances the presence of ferritin, hemosiderin and deoxyhemoglobin
- Exquisite images to diagnose microbleeds and abnormal oxygenation levels

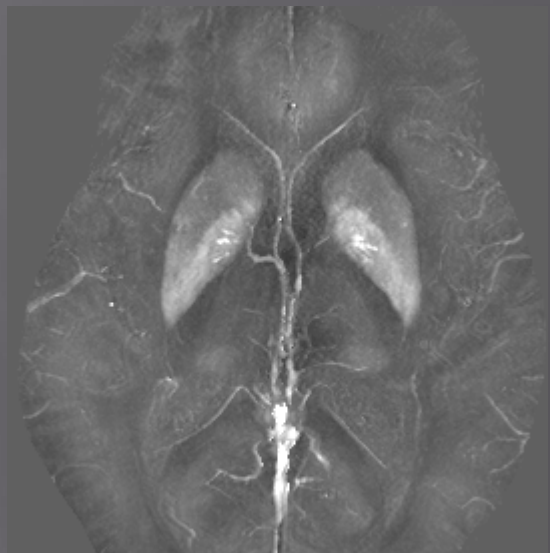
Normal volunteer



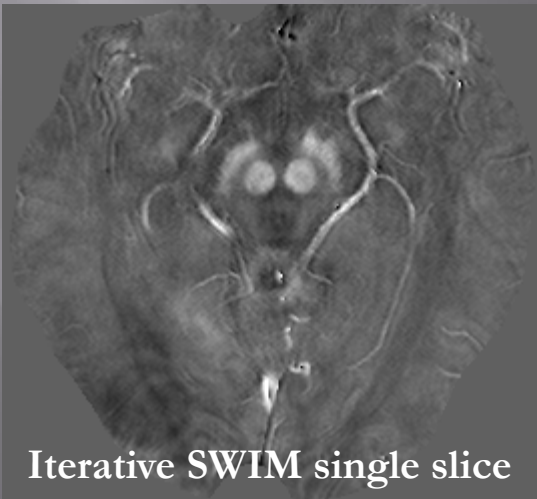
Iterative SWIM single slice



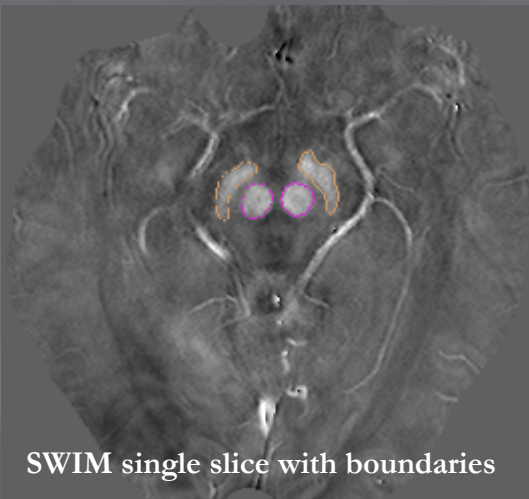
SWIM single slice with boundaries



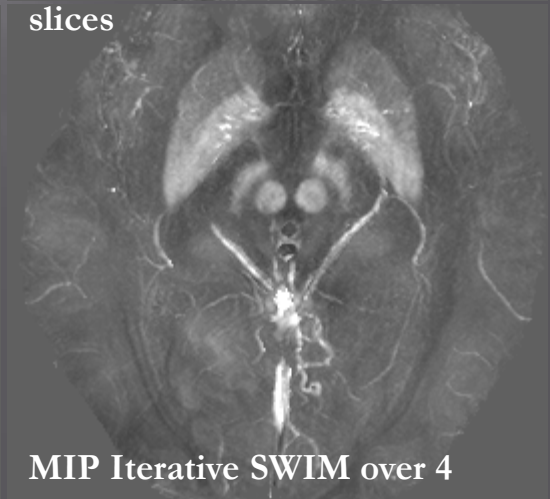
MIP Iterative SWIM over 4 slices



Iterative SWIM single slice

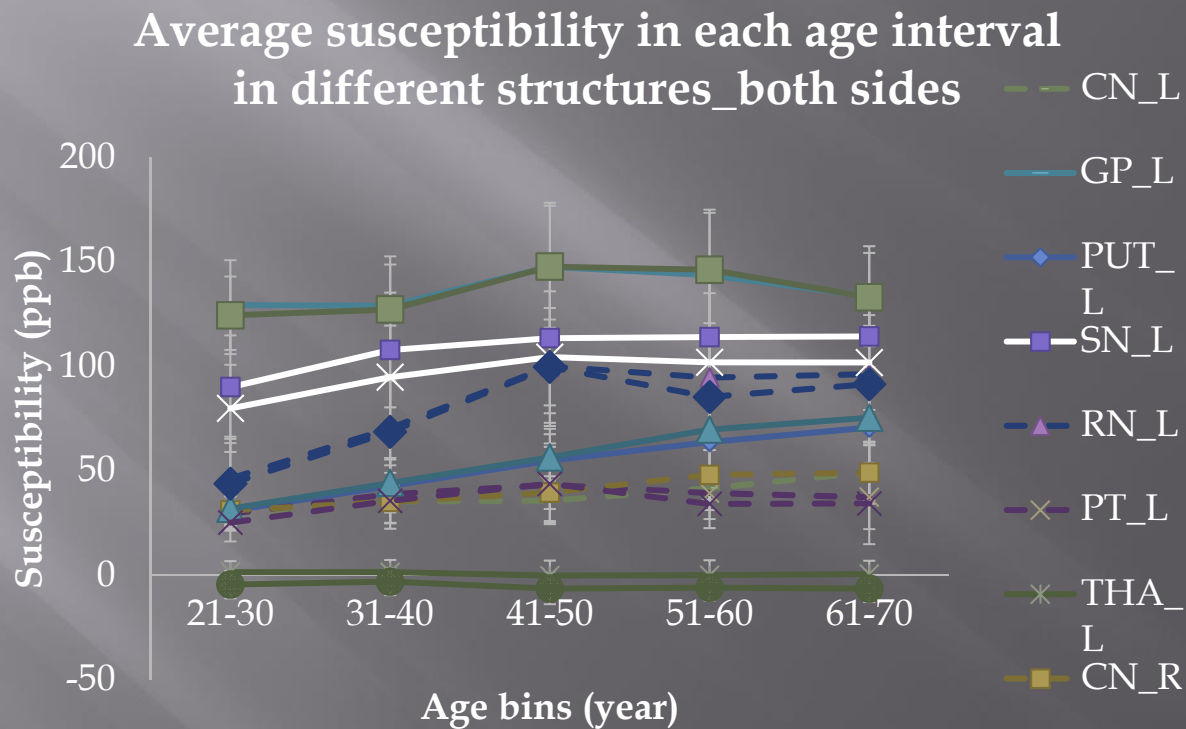


SWIM single slice with boundaries



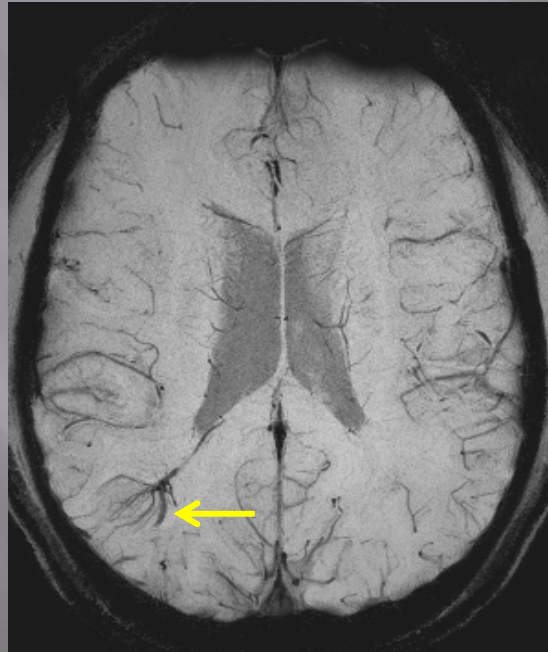
MIP Iterative SWIM over 4 slices

We all rust as we get older

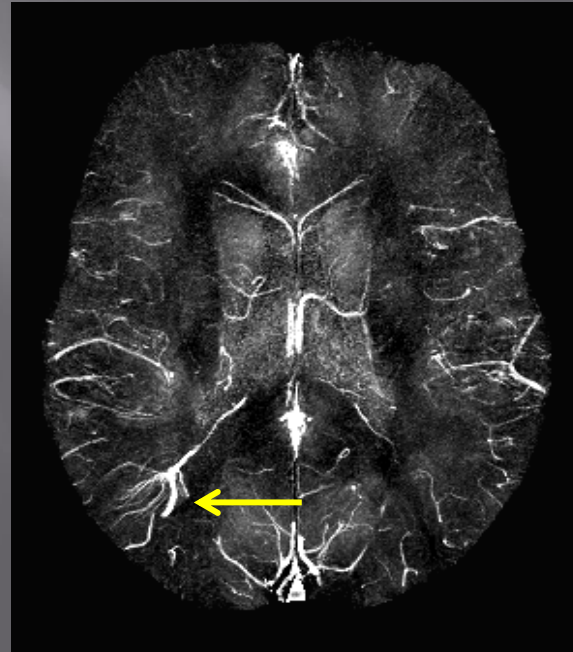


Deep venous anomaly in a healthy control

SWI

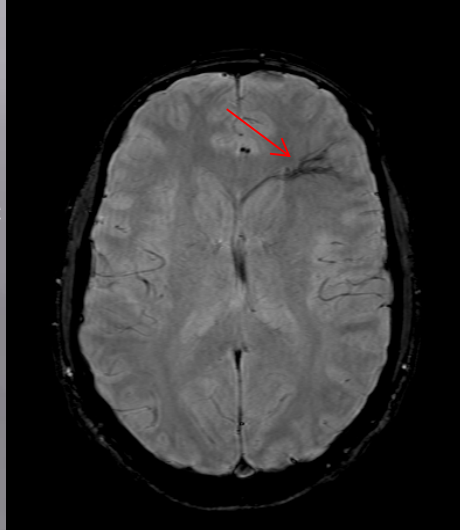


SWIM

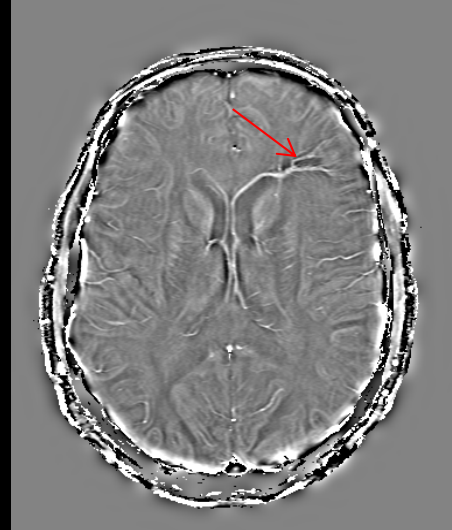


SWI reveals MVD

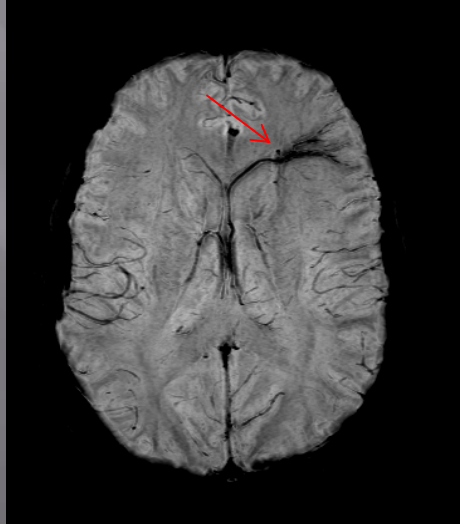
SWI-Magnitude



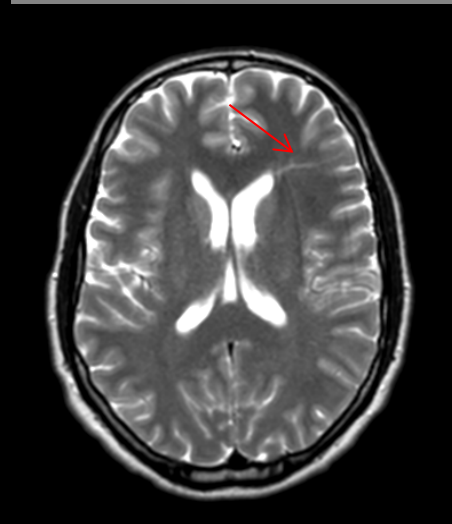
SWI-Phase



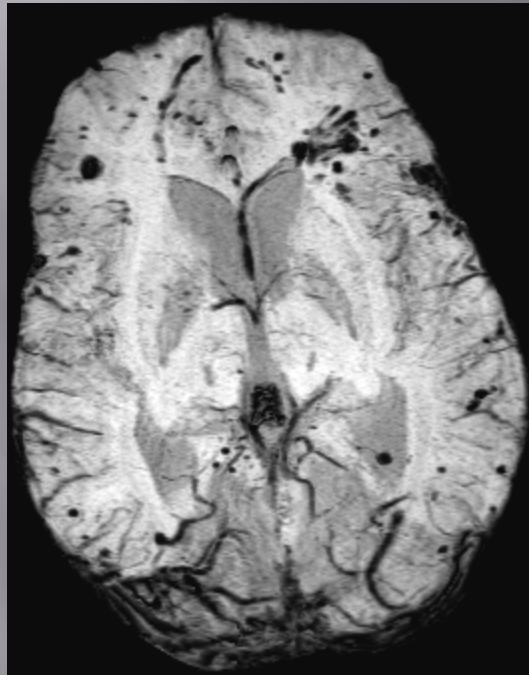
SWI-mIP



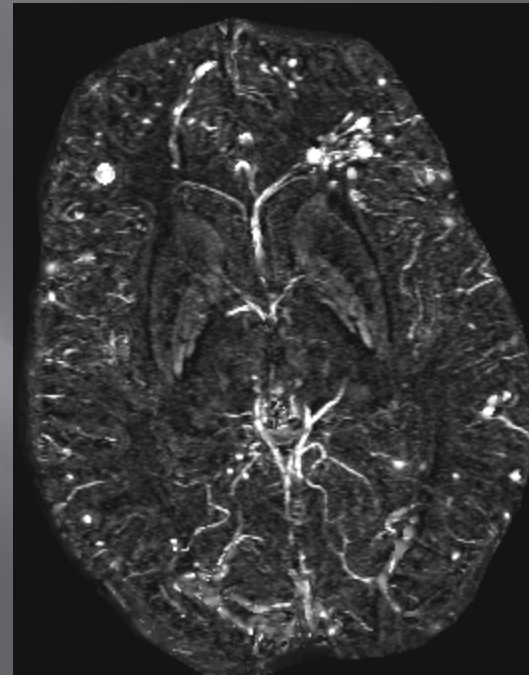
T2



The First Clinical Applications of SWIM in Traumatic Brain Injury (TBI)



SWI minIP image projected
over 16mm



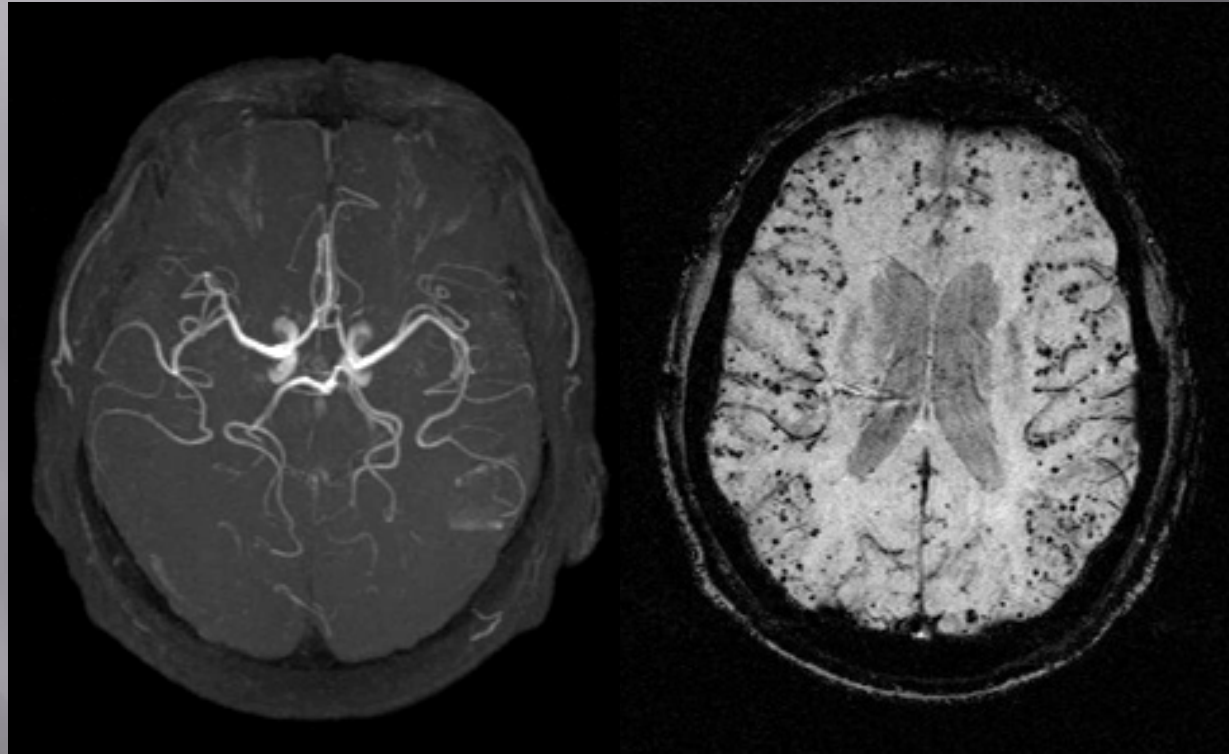
Corresponding MaxIP
susceptibility map image
projected over 16mm

**Cerebral Microbleeds: Pathophysiology to Clinical Practice (Cambridge
Medicine) Editor, David J. Werring, 2011, ISBN-13: 9780521198455**

Imaging Aging

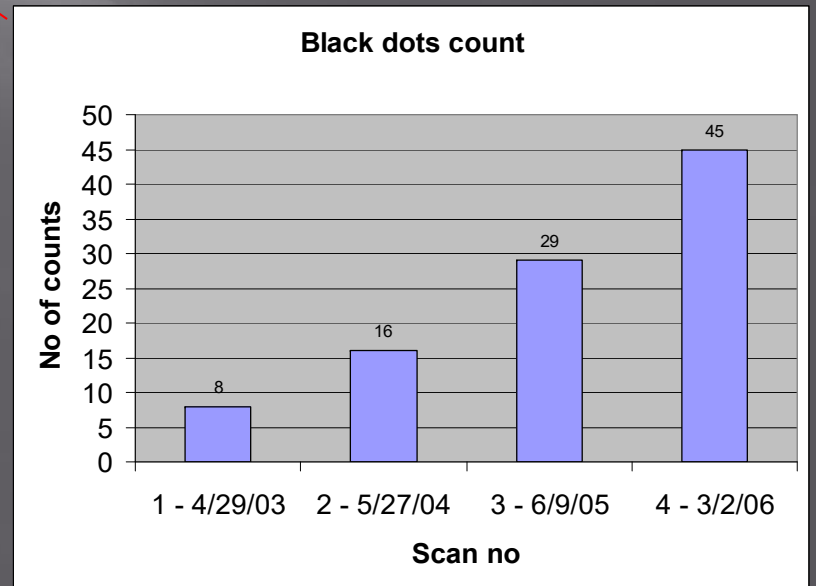
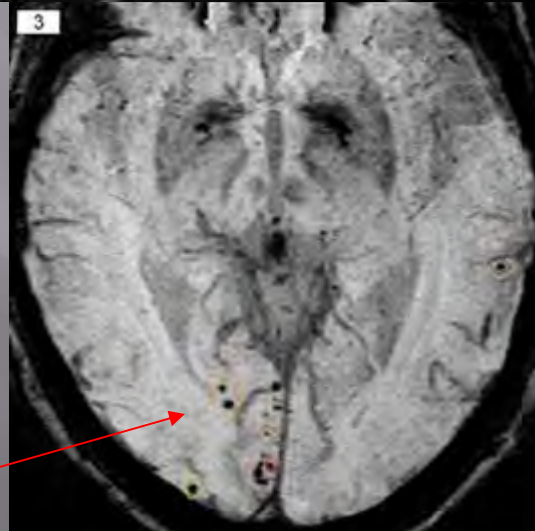
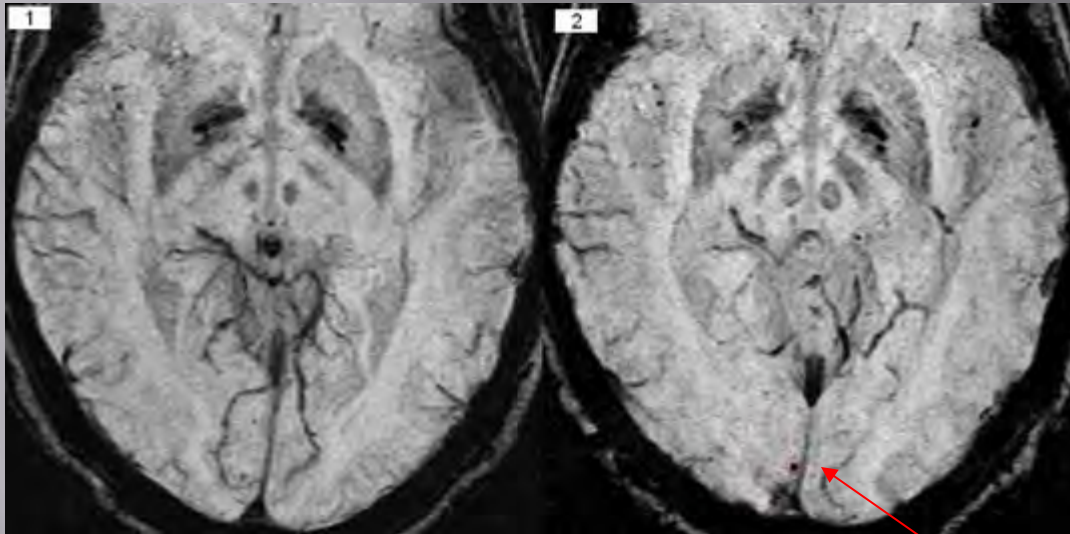
- ▶ It is now believed that up to 35% of dementia cases may be caused by vascular dementia.
- ▶ We see microhemorrhages as a means to predict who will get Alzheimer's disease.
- ▶ These may lead to “cognitive strokes”.
- ▶ Hopefully this work will lead to collaborations with the pharmaceutical industry to come up with neuroprotective drugs that will strengthen the vessel wall or help to prevent its degeneration.

Cerebral amyloid angiopathy



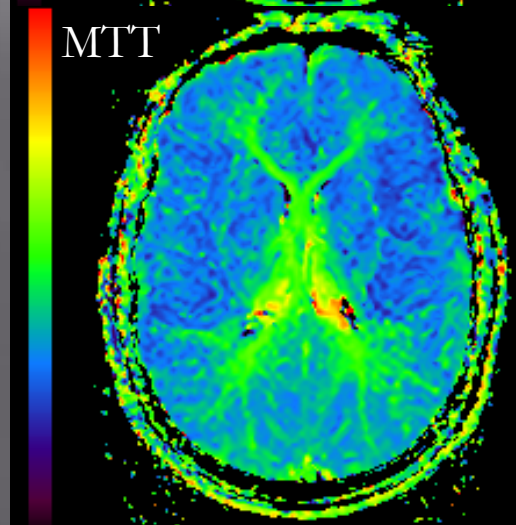
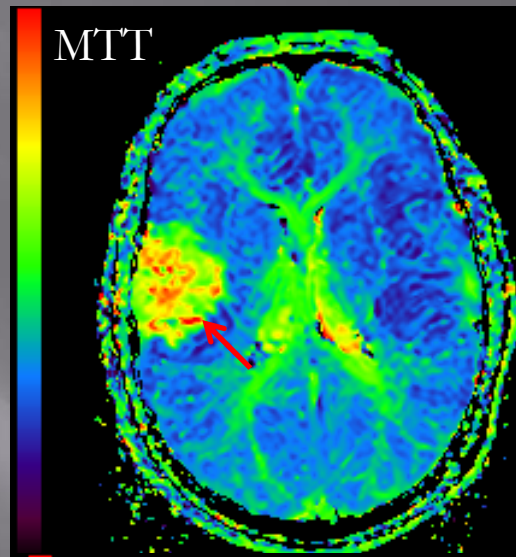
50 μ objects can manifest as 1mm³ objects

time to go sailing



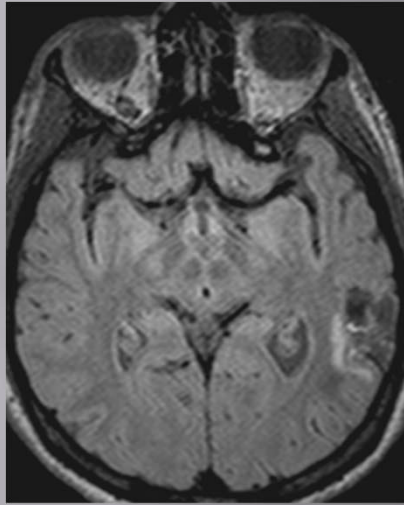
Two scans from same stroke patient

MRI scan date: 2013.01.04

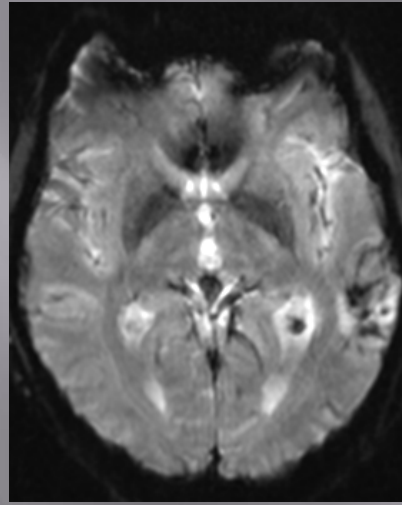


MRI scan date: 2013.01.11

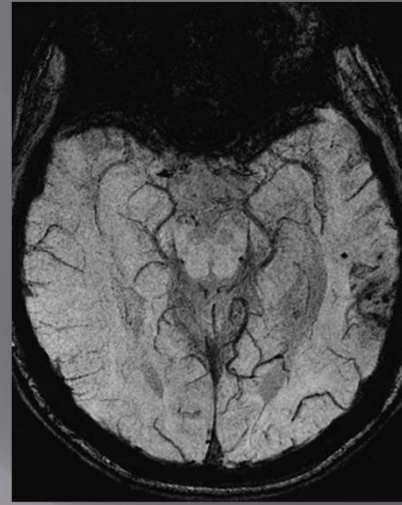
Stroke case for a young woman in her mid 30s



FLAIR



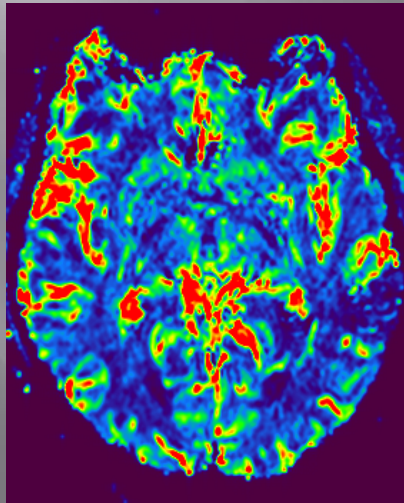
PWI (1st)



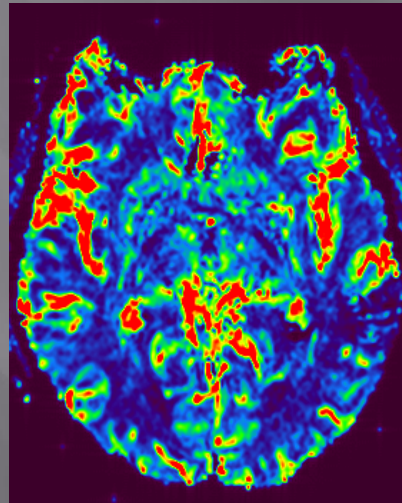
SWI mIP



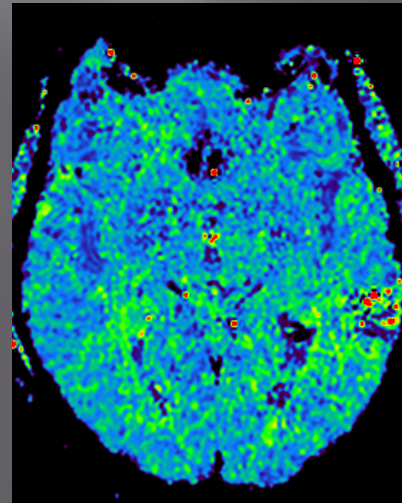
MRA



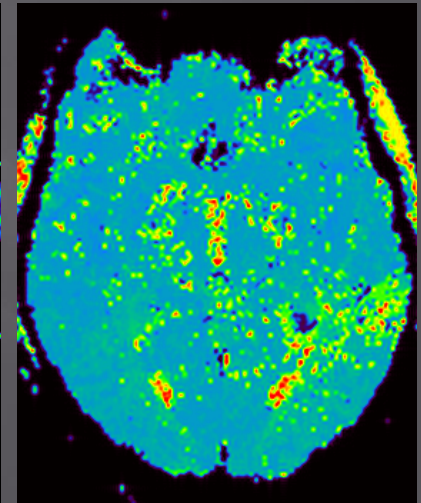
CBV



CBF



MTT



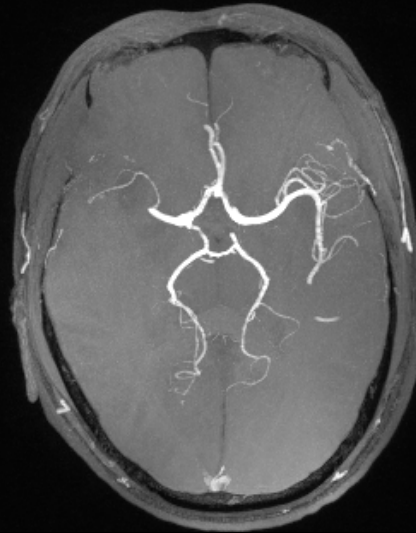
TTP

Imaging veins and arteries using double echo SWI⁵ Images courtesy of Meiyun Wang, Zhengzhou

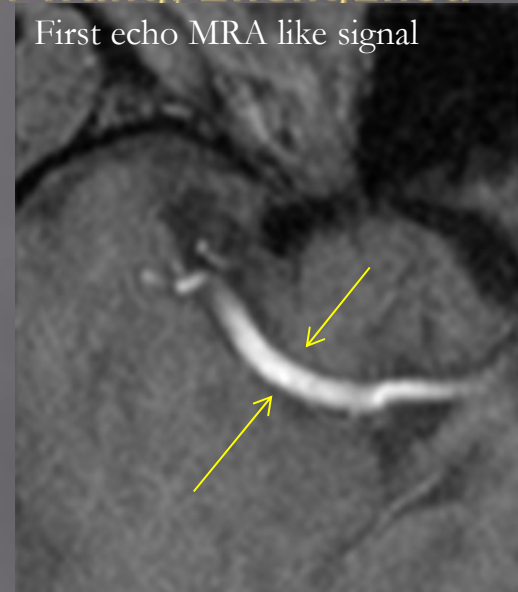
Thrombus dominates the SWI image (TE = 7.5ms)



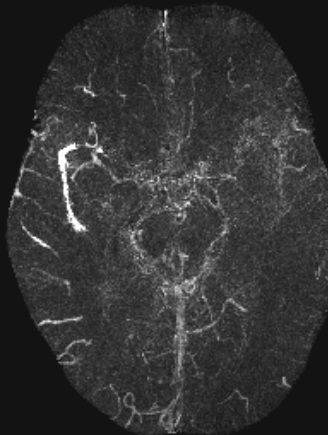
First echo MIP



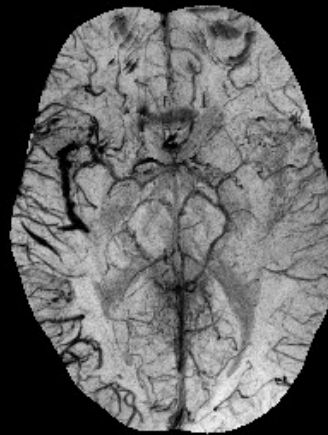
First echo MRA like signal



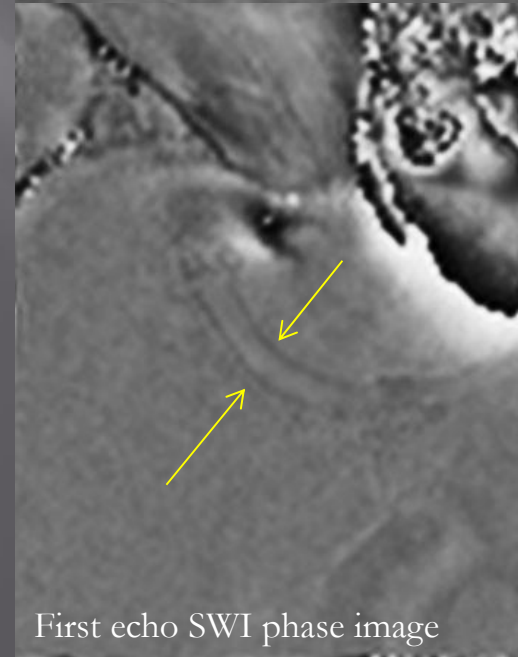
Thrombus dominates the SWIM image (TE = 7.5ms)



Second echo (17.5ms) true SWI



Note the asymmetrically prominent cortical veins



First echo SWI phase image

Using caffeine decreases blood flow to the brain

two cups of coffee and you will have a major change of blood flow to the brain

maybe we should approach Starbucks for funding

at least it is a relatively harmless contrast agent to use to study the brain and a heck of a lot cheaper

SWI as a high resolution BOLD imaging method

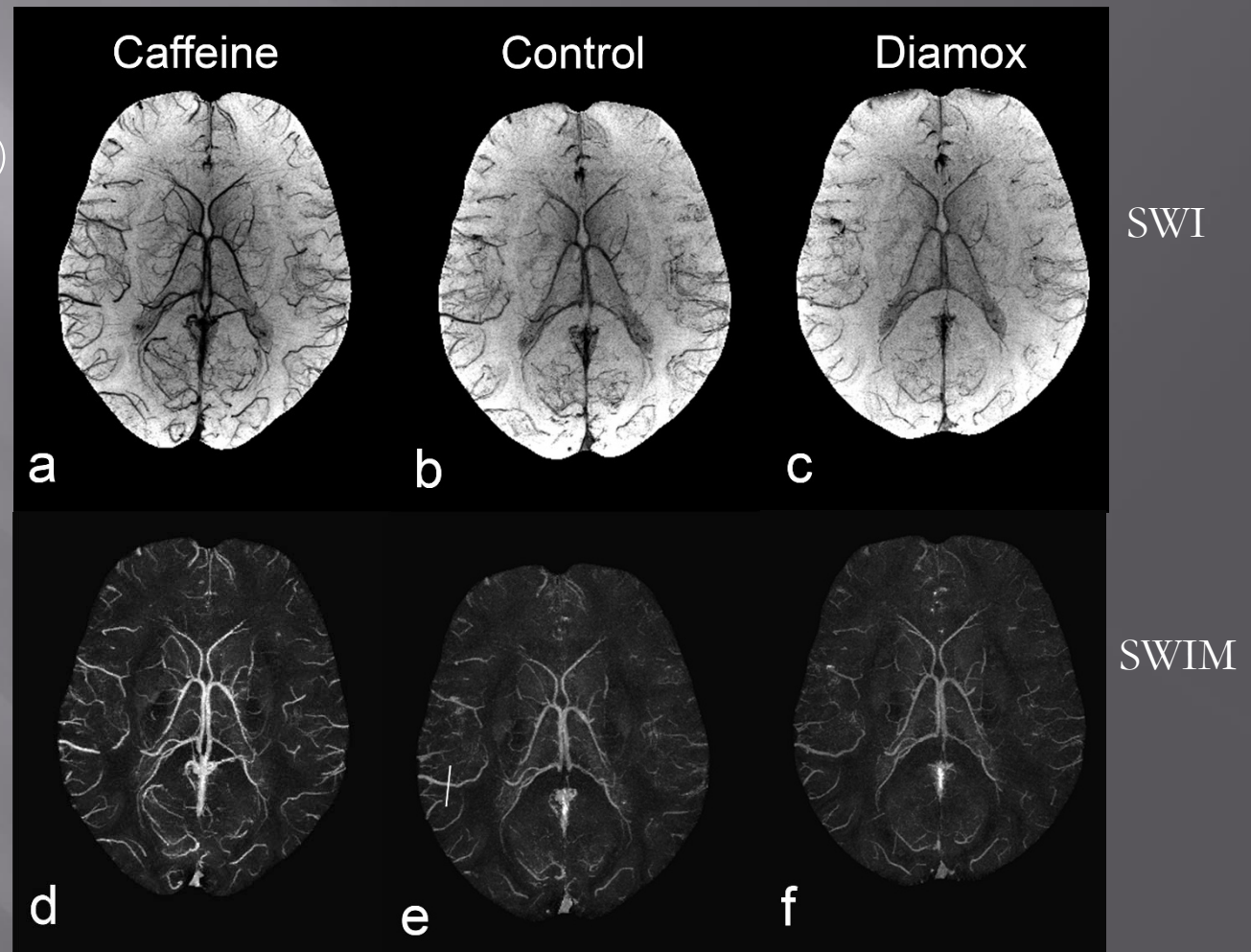


MinIP of caffeine/Gd over 28 slices with 4 phase multiplications

Imaging veins and blood products using SWI and SWIM: Challenging the neurovascular system⁴

200mg caffeine pills (a, d)
or 1000mg diamox IV
injection (c, f).

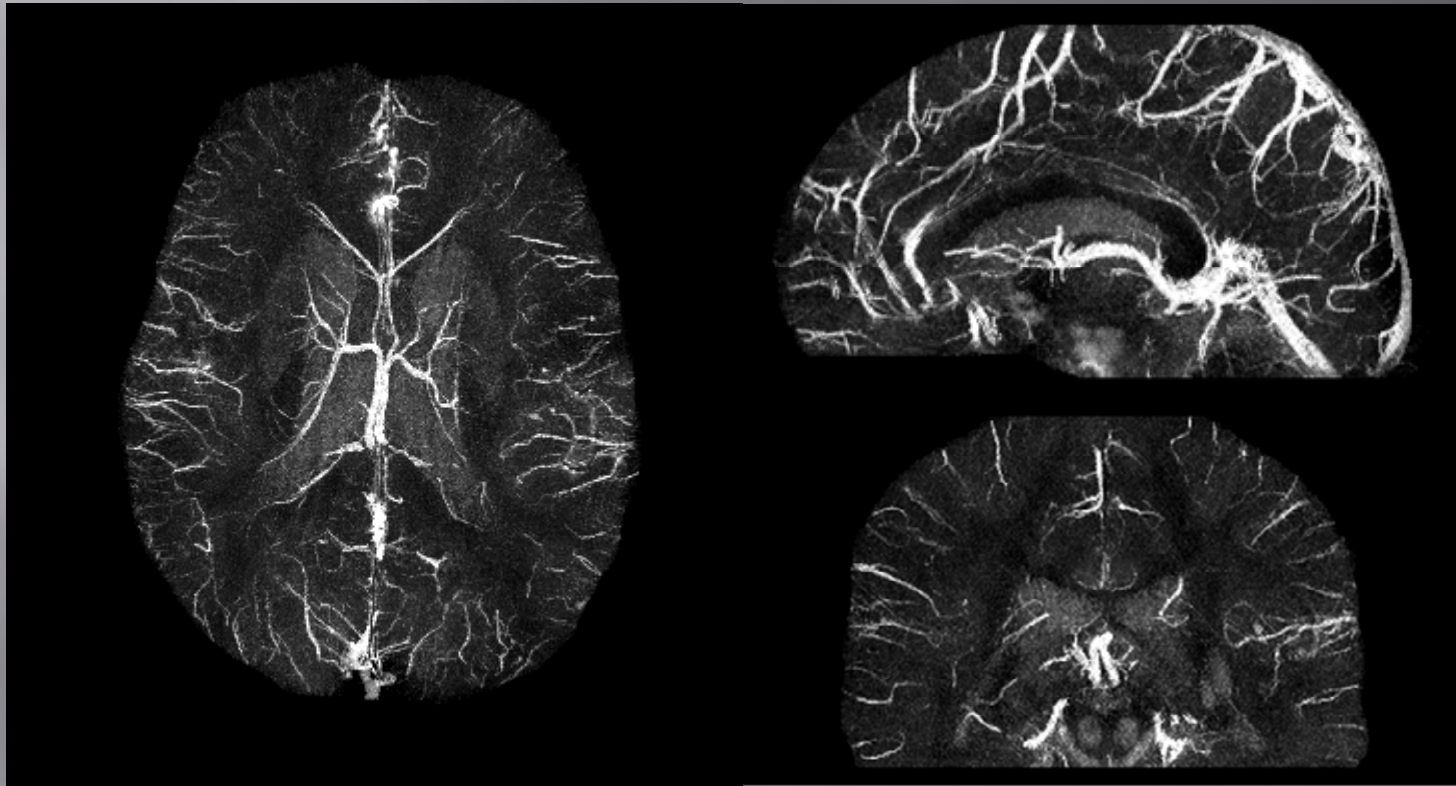
Compared to the control
condition (b,e),
significant oxygen
saturation changes are
observed post-challenge
on veins throughout the
brain.



Caffeine: flow change = $-27\% \pm 9\%$ and $\Delta Y = -0.09 \pm 0.02$

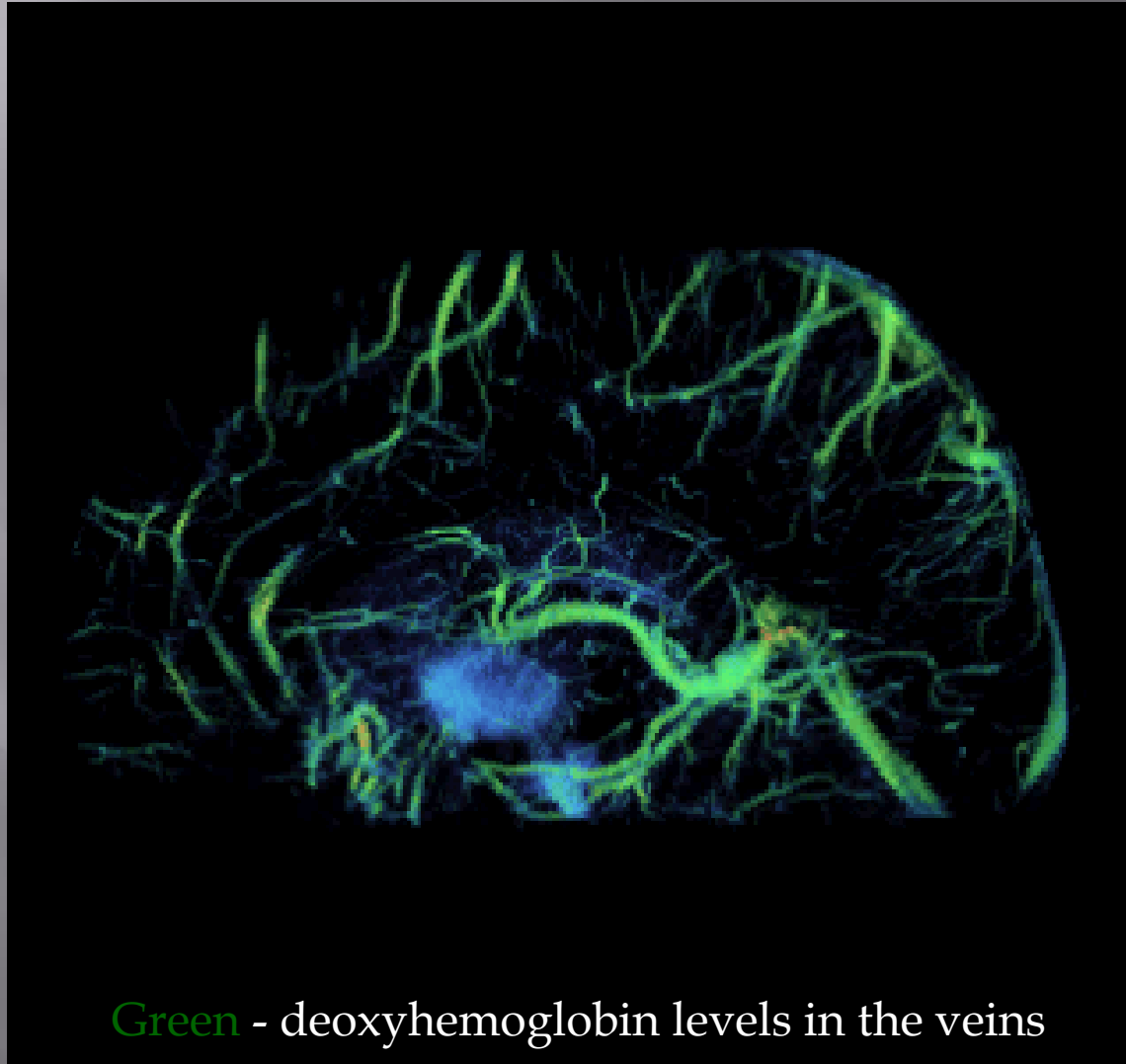
Diamox: flow change = $+40\% \pm 7\%$ and $\Delta Y = +0.10 \pm 0.01$

Future Directions: OXYGEN EXTRACTION FRACTION



MIPs of SWIM data over 8mm. The data were collected at 3T with TE=14.3ms and a voxel size $0.5 \times 0.5 \times 0.5 \text{mm}^3$.

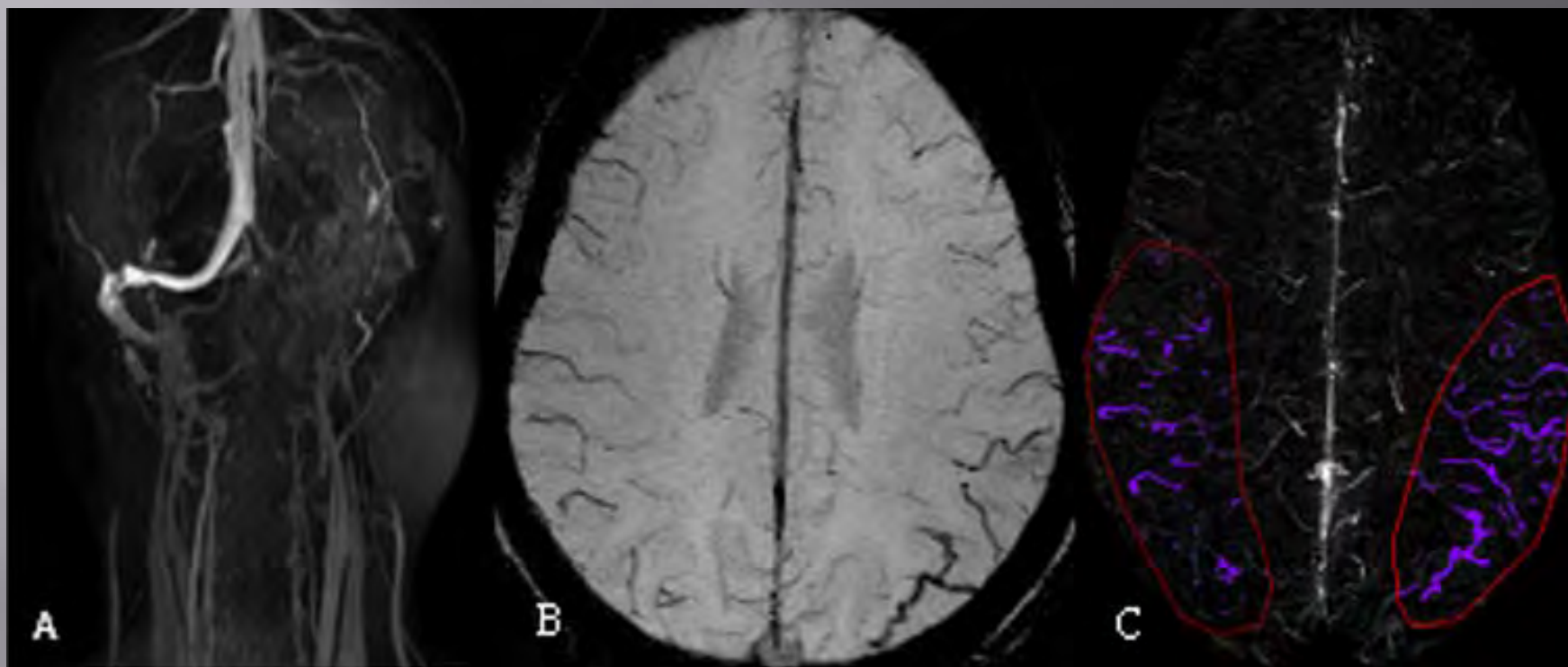
Whole brain iron oxygen extraction fraction



Green - deoxyhemoglobin levels in the veins

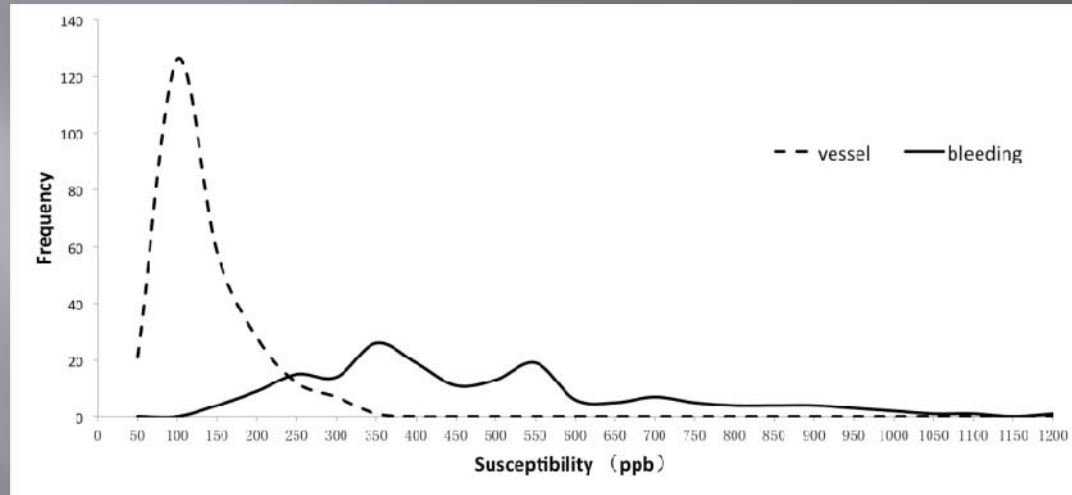
Blue represents iron in the basal ganglia and midbrain

Headache can be associated with bad venous vasculature



A 32-year-old female with headache and intracranial hypertension. Occlusion of the left transverse sinus (CE MRAV, A) and APCVs on the mIPped-SWI images (B). The susceptibility value of the ipsilateral pial veins measured 159 ± 60 ppb and the contralateral measured only (131 ± 43) ppb.

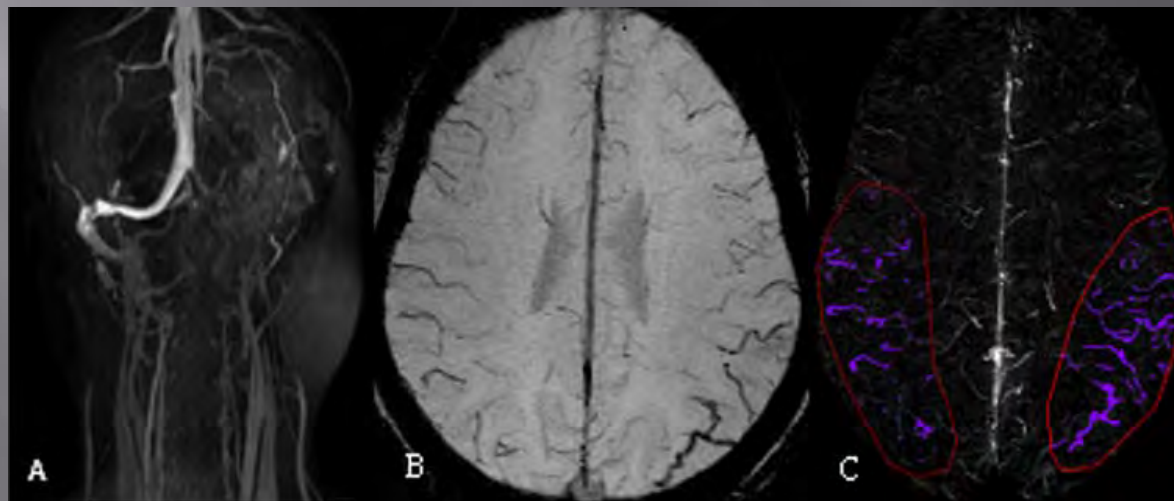
Stroke: Isolating poor flow using a threshold in SWIM^{9,10}



Imaging headache and idiopathic intracranial hypertension

Asymmetrically prominent cortical veins are seen bilaterally

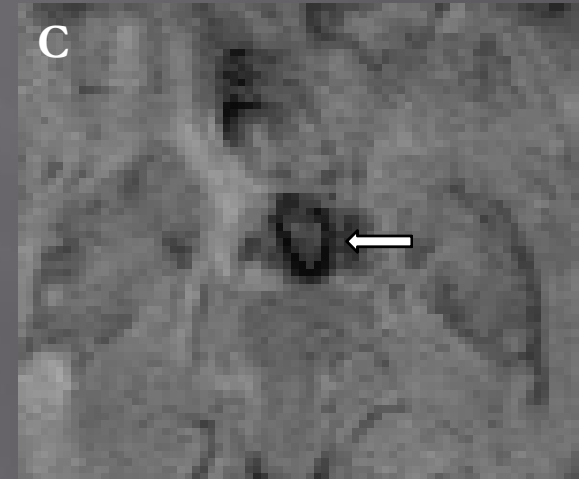
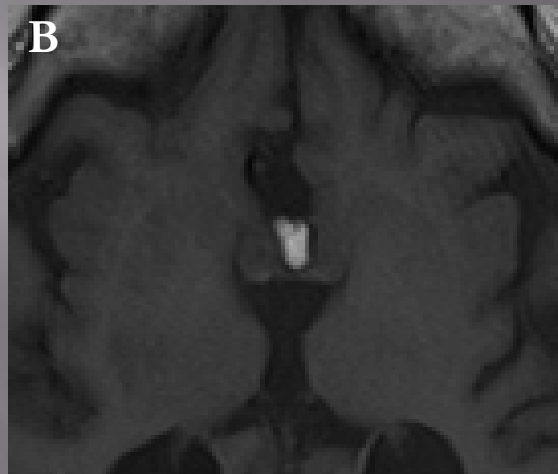
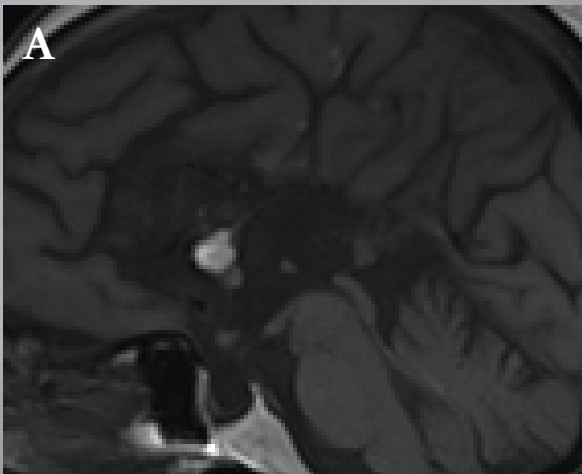
Abnormal dural sinuses and jugular vein



Fat containing intracranial lesions

- Congenital lesions
- Lipoma
- Dermoid
- Tumor
- Teratoma
- Craniopharyngioma
- Lipomatous meningioma
- Lipomatous differentiation/transformation of PNETs, ependymoma and glioma.
- Cerebellar liponeurocytoma
- Acquired
- Dissemination of fat in CSF after skull base/fat graft surgery.

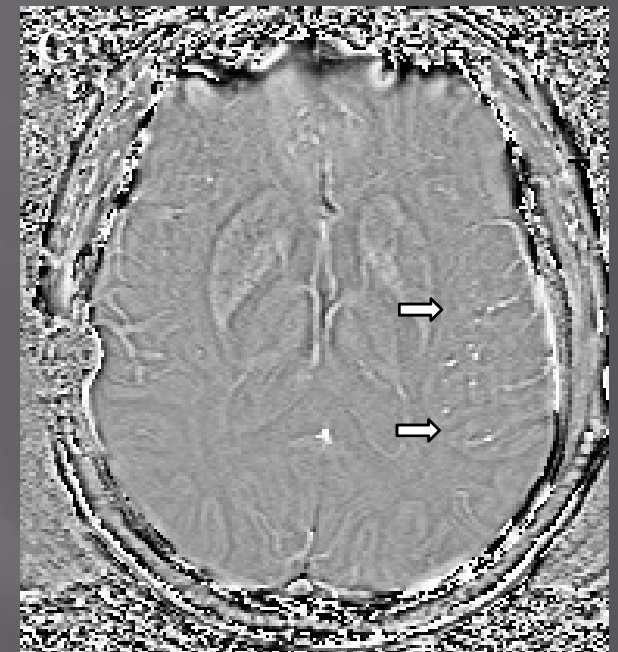
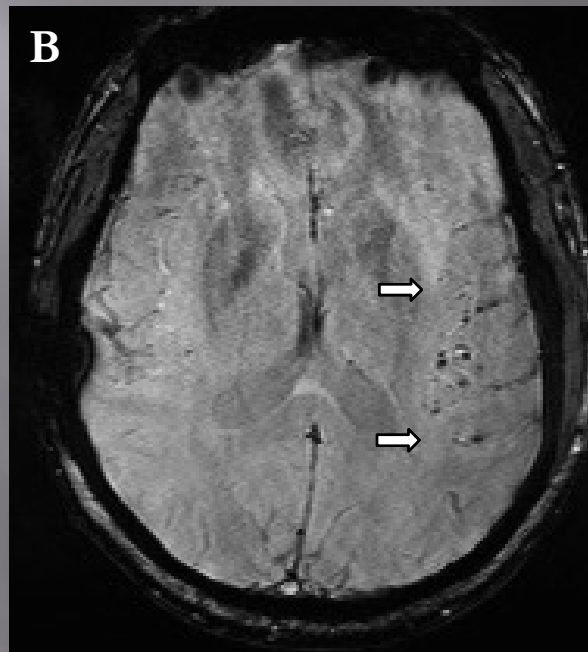
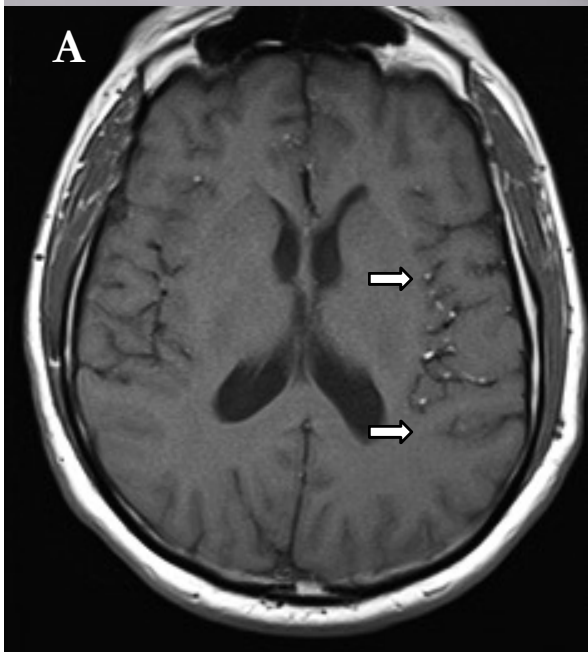
Callosal Lipoma



35-year-old male with an anterior interhemispheric lipoma in association with corpus callosum agenesis. MRI brain sagittal (A) and axial (B) T1WI depict the lipoma as a T1 hyperintense lesion located in the anterior interhemispheric fissure. SWI (C) shows a hypointense rim (arrow) surrounding the lipoma which represents the chemical artifact at the fat-CSF interface.

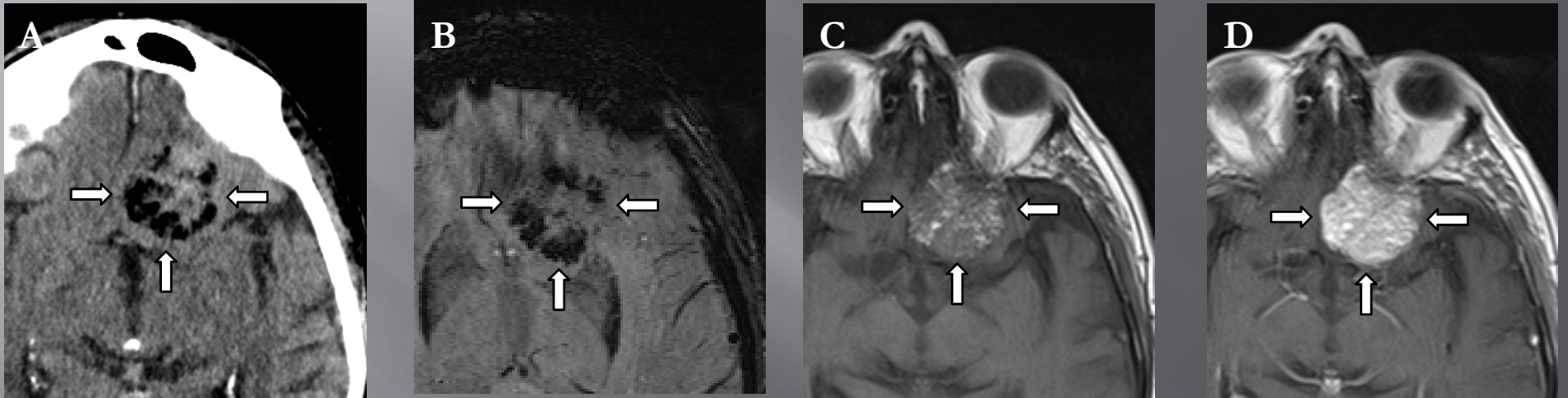
Images courtesy of Charles Hsu
AJR Am J Roentgenol 2013;201:902-7

Ruptured Dermoid Cyst



42-year-old man with ruptured intracranial dermoid. MRI brain T1WI (A) shows multiple small T1 hyperintense tiny fat droplets in the subarachnoid space of the left Sylvian fissure. On SWI (B) the fat droplets appear hypointense. Phase image (C) depicts the tiny fat droplets as hyperintense foci. Left handed MRI system, Siemens.

Lipomatous meningioma



78-year-old male with a left sphenoid ridge lipomatous meningioma. CT head (A) shows a fat containing extra-axial mass (arrows) with central area of soft tissue density. MRI brain SWI (B) depicts the peripheral areas of fat attenuation as hypointense. T1WI (C) confirms high signal intensity in areas of intralesional fat. Post gadolinium enhanced T1WI (D) shows homogenous enhancement pattern.

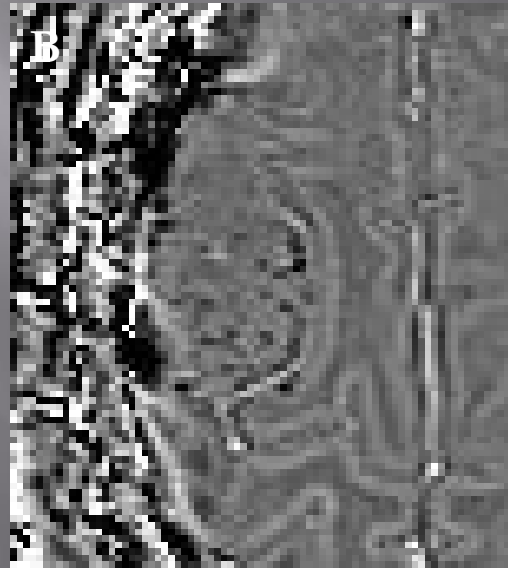
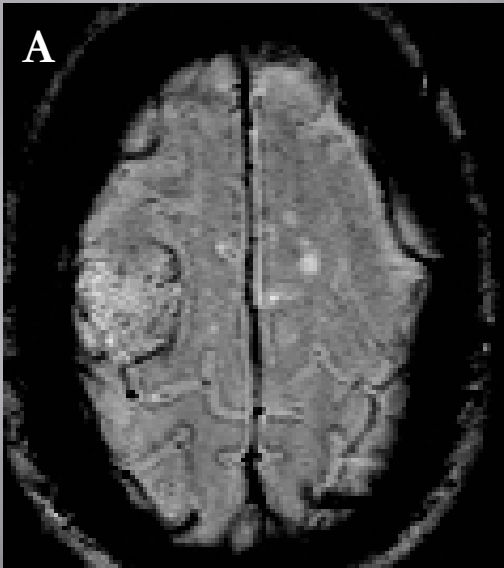
Intratumoral Susceptibility Signal

Intratumoral Susceptibility Signal describes the intratumoral susceptibility signal characteristics, which may be due to microhaemorrhage, neoangiogenesis or **calcification**.

Phase shift in calcified intracranial neoplasm

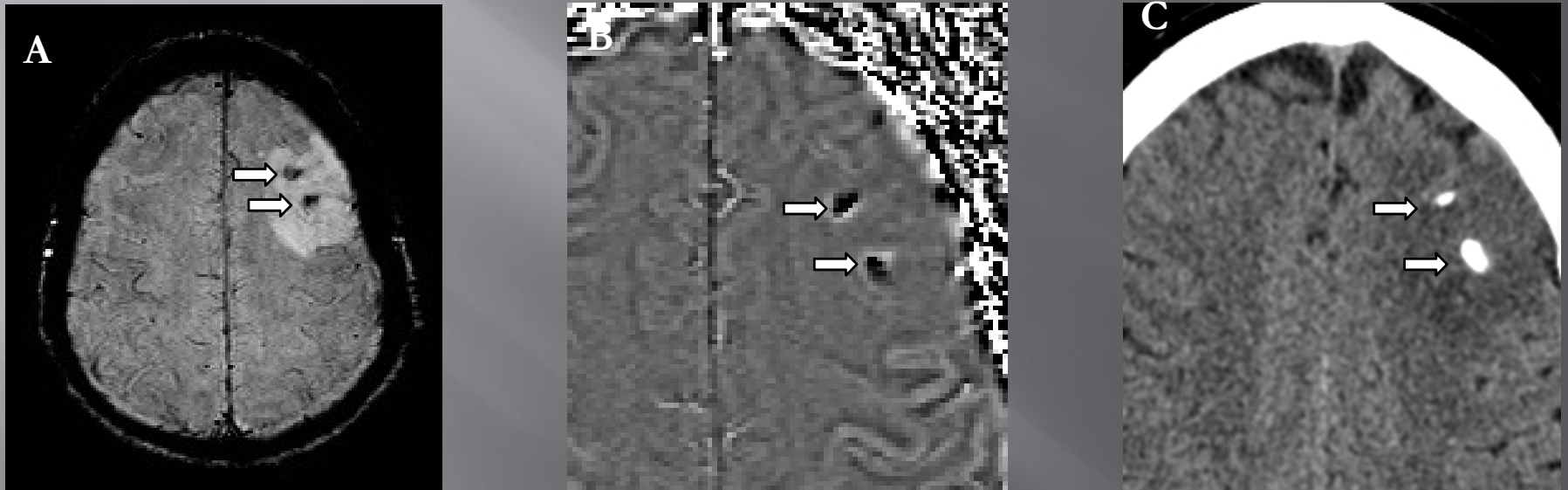
- Heme iron and calcium generate opposing phase shift values on the SWI phase image.
- Diamagnetic substances such as calcium demonstrate negative shift on phase imaging, however, paramagnetic substances such as deoxyhemoglobin, hemosiderin and ferritin demonstrate positive shift on phase imaging for a left handed system.

Meningioma



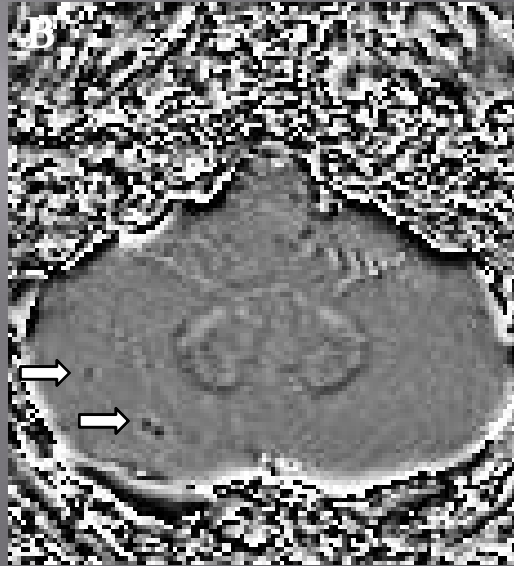
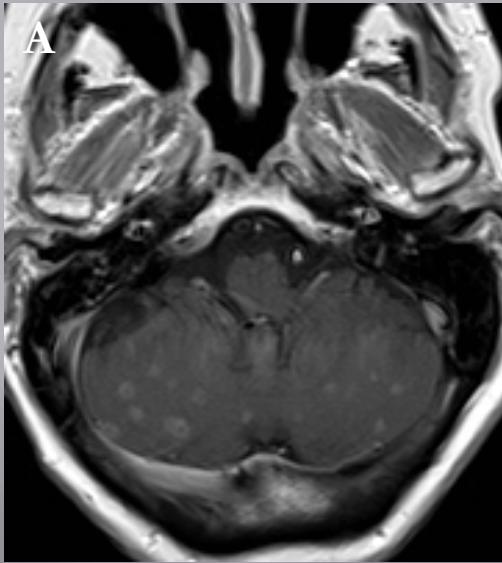
42-year-old female with a right frontal meningioma. MRI brain SWI (A) depicts an extra-axial mass with hypointense intralésional foci. On the phase image (B) these intralésional foci appear hypointense suggestive of intralésional calcifications. CT head (C) confirms punctate intralésional calcifications. Left handed MRI system, Siemens.

Oligodendroglioma (WHOII)



40-year-old female patient with a left frontal oligodendroglioma. SWI image (A) shows two punctate hypointense foci (arrows) which are also hypointense on the phase image (B) confirming intratumoral calcifications. Corresponding non-contrast CT (C) confirms the presence of intratumoral calcifications. Left handed MRI system, Siemens.

Calcified Metastases

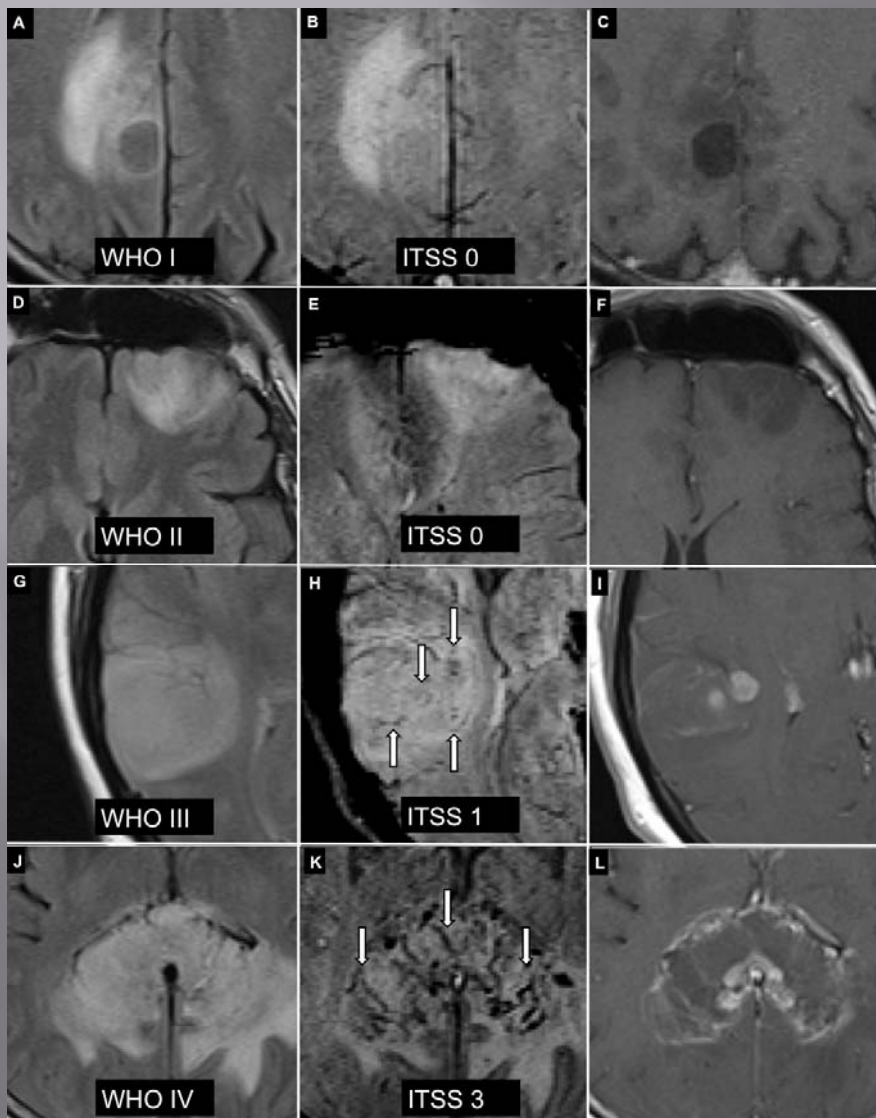


50 year-old female with calcified cerebral metastases from breast cancer. Post contrast T1WI (A) shows multiple enhancing lesions in the cerebellum. Phase image (B) show some of the lesion as hypointense (arrows). Corresponding non-contrast CT (C) confirms multiple calcified lesions which were underestimated on the phase image. (Images acquired on the left handed MRI system, Siemens).

Intratumoral Susceptibility Signal

Intratumoral Susceptibility Signal describes the intratumoral susceptibility signal characteristics, which may be due to **microhaemorrhage, neoangiogenesis** or calcification.

ITSS and Histological Grading of Glioma



Research has shown a reliable correlation of ITSS with tumoral vascularity on dynamic susceptibility-weighted contrast-enhanced (DSC) perfusion-weighted MRI (PWI) and histological grade (WHO).

The ITSS grading scheme is as follows:

Grade 0: no ITSS

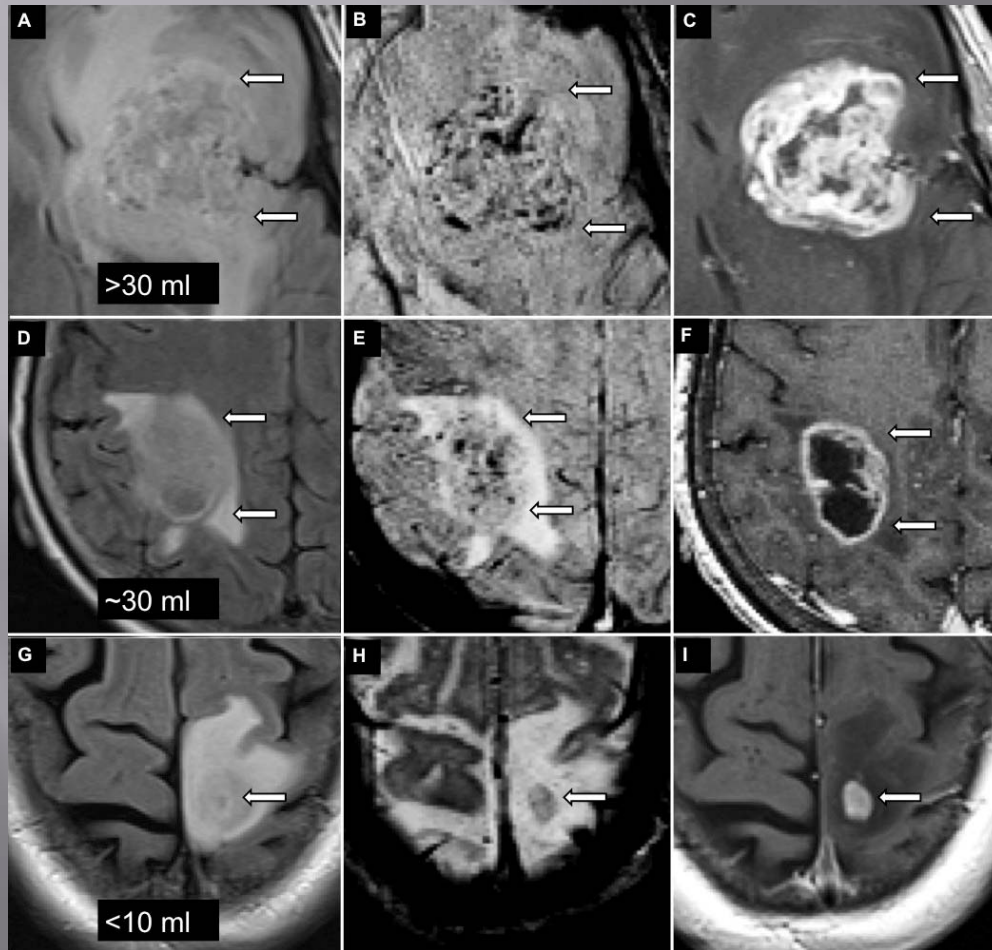
Grade 1: 1–5 dot-like or fine linear ITSSs

Grade 2: 6–10 dot-like or fine linear ITSSs

Grade 3: 11 dot-like or fine linear ITSSs

J Magn Reson Imaging 2014 ;39:1569-74

ITSS and Volume of Glioblastoma



Example of relationship between tumoral volume of glioblastoma and ITSS grade. Glioblastomas with > 30 ml volume (A-C) demonstrate greater ITSS in comparison with moderate volume ~ 30 ml glioblastomas (D-F). Smaller glioblastomas < 10 ml volume (G-I) demonstrate minimal ITSS. (Images acquired on the left handed MRI system, Siemens).

Conclusions

MR can provide information on:

- Arteries and Veins separately
- Microvasculature
- Oxygen saturation

Can this capability be used to better image tumors?